

Supporting Information for

**Anomalously Enhanced Ion Transport and Uptake in Functionalized Angstrom-scale  
Two-dimensional Channels**

Mingzhan Wang<sup>a</sup>, Tumpa Sadhukhan<sup>b,c</sup>, Nicholas H. C. Lewis<sup>d</sup>, Maoyu Wang<sup>e</sup>, Xiang He<sup>f,1</sup>,  
Gangbin Yan<sup>a</sup>, Dongchen Ying<sup>a</sup>, Eli Hoenig<sup>a</sup>, Yu Han<sup>a</sup>, Guiming Peng<sup>a,2</sup>, One-Sun Lee<sup>b</sup>,  
Fengyuan Shi<sup>g</sup>, David M. Tiede<sup>f</sup>, Hua Zhou<sup>e</sup>, Andrei Tokmakoff<sup>d</sup>, George C. Schatz<sup>b,3</sup>,  
Chong Liu<sup>a,3</sup>

- a. Pritzker School of Molecular Engineering, University of Chicago, Chicago, IL 60637, USA.
- b. Department of Chemistry, Northwestern University, Evanston, Illinois 60208, USA.
- c. Department of Chemistry, SRM Institute of Science and Technology, Kattankulathur, Tamil Nadu, 603203, India
- d. Department of Chemistry, Institute for Biophysical Dynamics, and James Franck Institute, University of Chicago, Chicago, IL 60637, USA.
- e. X-Ray Science Division, Advanced Photon Source, Argonne National Laboratory, Lemont, IL 60439, USA.
- f. Advanced Materials for Energy-Water Systems (AMEWS) Energy Frontier Research Center and Chemical Sciences and Engineering Division, Argonne National Laboratory, Lemont, IL 60439, USA.
- g. Electron Microscopy Core, University of Illinois Chicago, Chicago, IL 60607, USA.

- 1 Present Address: Department of Mechanical and Civil Engineering, Florida Institute of Technology, Melbourne, FL 32901, USA
- 2 Present Address: College of Chemistry and Chemical Engineering, Jiangxi Normal University, Nanchang, Jiangxi 330022, China
- 3 To whom correspondence may be addressed.

Email: [✉ g-schatz@northwestern.edu](mailto:g-schatz@northwestern.edu) or [✉ chongliu@uchicago.edu](mailto:chongliu@uchicago.edu).

## **Materials and Methods**

### **Supplementary Text**

#### **Figs. S1 to S24**

#### **Tables S1 to S4**

#### **Supplementary References 32-46**

## **Materials and Methods**

### **Preparation of mixed ions solution**

(A) Mixed ions solution with dominant chloride anions ( $\text{Cl}^-/\text{NO}_3^- \approx 96:44$ ):  
 $\text{KCl}/\text{NaCl}/\text{LiCl}/\text{MgCl}_2/\text{AlCl}_3/\text{CaCl}_2 \cdot 2\text{H}_2\text{O}/\text{BaCl}_2 \cdot 2\text{H}_2\text{O}/\text{CoCl}_2 \cdot 6\text{H}_2\text{O}/\text{CuCl}_2 \cdot 2\text{H}_2\text{O}/\text{MnCl}_2 \cdot 4\text{H}_2\text{O}/\text{CdCl}_2/\text{NiCl}_2/\text{ZnCl}_2/\text{Y}(\text{NO}_3)_3 \cdot 6\text{H}_2\text{O}/\text{La}(\text{NO}_3)_3 \cdot 6\text{H}_2\text{O}/\text{Yb}(\text{NO}_3)_3 \cdot 5\text{H}_2\text{O}/\text{Pb}(\text{NO}_3)_2$  were used as salts. In this case, the ratio  $\text{Cl}^-/\text{NO}_3^- \approx 96:44$ .

(B) Mixed ions solution with pure nitrate ( $\text{NO}_3^-$ ) anions:  
 $\text{KNO}_3/\text{NaNO}_3/\text{LiNO}_3/\text{Mg}(\text{NO}_3)_2 \cdot 6\text{H}_2\text{O}/\text{Al}(\text{NO}_3)_3 \cdot 9\text{H}_2\text{O}/\text{Ca}(\text{NO}_3)_2 \cdot 4\text{H}_2\text{O}/\text{Ba}(\text{NO}_3)_2 \cdot 6\text{H}_2\text{O}/\text{Co}(\text{NO}_3)_2 \cdot 6\text{H}_2\text{O}/\text{Ni}(\text{NO}_3)_2 \cdot 6\text{H}_2\text{O}/\text{Cu}(\text{NO}_3)_2 \cdot 2.5\text{H}_2\text{O}/\text{Mn}(\text{NO}_3)_2 \cdot 4\text{H}_2\text{O}/\text{Zn}(\text{NO}_3)_2 \cdot 6\text{H}_2\text{O}/\text{C}$

$\text{d}(\text{NO}_3)_2 \cdot 4\text{H}_2\text{O}/\text{Y}(\text{NO}_3)_3 \cdot 6\text{H}_2\text{O}/\text{La}(\text{NO}_3)_3 \cdot 6\text{H}_2\text{O}/\text{Yb}(\text{NO}_3)_3 \cdot 5\text{H}_2\text{O}/\text{Pb}(\text{NO}_3)_2$  were used as salts.

$\text{KNO}_3 (\geq 99\%)$ ,  $\text{NaNO}_3 (> 99\%)$ ,  $\text{Mg}(\text{NO}_3)_2 \cdot 6\text{H}_2\text{O}$  (99%),  $\text{Ca}(\text{NO}_3)_2 \cdot 4\text{H}_2\text{O} (\geq 99\%)$ ,  $\text{Co}(\text{NO}_3)_2 \cdot 6\text{H}_2\text{O}$  (98%),  $\text{Cu}(\text{NO}_3)_2 \cdot 2.5\text{H}_2\text{O}$  (98%),  $\text{Zn}(\text{NO}_3)_2 \cdot 6\text{H}_2\text{O}$  (98%),  $\text{Cd}(\text{NO}_3)_2 \cdot 6\text{H}_2\text{O}$  ( $> 99\%$ ),  $\text{Pb}(\text{NO}_3)_2 (> 99\%)$ ,  $\text{NaCl}$  (99.5%),  $\text{AlCl}_3$  (99.99%),  $\text{CaCl}_2 \cdot 2\text{H}_2\text{O} (\geq 99\%)$   $\text{MnCl}_2 \cdot \text{CoCl}_2 \cdot 6\text{H}_2\text{O}$  (98%) were purchased from Sigma-Aldrich.  $\text{LiNO}_3$  (99+%),  $\text{CdCl}_2$  (99%) were purchased from ACROS Organics.  $\text{Ba}(\text{NO}_3)_2$  (99.999%),  $\text{Mn}(\text{NO}_3)_2 \cdot 4\text{H}_2\text{O}$  (98%),  $\text{KCl}$  (99.0-100.5%),  $\text{MgCl}_2$  (99%),  $\text{CuCl}_2 \cdot 2\text{H}_2\text{O}$  (99%) and  $\text{ZnCl}_2$  (99.95%) were purchased from Alfa Aesar.  $\text{Al}(\text{NO}_3)_3 \cdot 9\text{H}_2\text{O}$  (98+%) was purchased from Strem Chemicals.  $\text{NiCl}_2$  (98%) was purchased from Fisher Scientific.  $\text{LiCl} (> 99\%)$  was purchased from Oakwook Chemicals.  $\text{Y}(\text{NO}_3)_3 \cdot 6\text{H}_2\text{O}$  (99+%),  $\text{La}(\text{NO}_3)_3 \cdot 6\text{H}_2\text{O}$  (99.99%) and  $\text{Yb}(\text{NO}_3)_3 \cdot 5\text{H}_2\text{O}$  (99.9%) were purchased from Neta Scientific Inc. All chemicals were used without further treatments.

Note: When preparing the mixture solution with chloride/nitrate anions, we observed that some salts cannot be dissolved  $\sim 25$  mM. Upon further dilution with DI water to  $\sim 10$  mM, we observed that all salts can be dissolved. The solubility issue set the upper bound of concentration. To guarantee that the light elements, e.g.  $\text{Li}^+$ , can be reliably detected by the ICPMS in the permeation test, we avoided a low concentration in the transport test, while we did the uptake test at  $\sim 0.4$  mM nonetheless (Figs. S15 and S16).

### **Preparation of $\text{MoS}_2$ -COOH dispersion solution**

First the single- or few-layer  $\text{MoS}_2$  nanosheet aqueous dispersion solution was prepared through the intercalation of  $\text{MoS}_2$  powders (Sigma-Aldrich)) in n-butyl lithium, as widely reported previously. Then the acetic acid functionalization of the  $\text{MoS}_2$  nanosheet was

achieved through its nucleophilic reaction with iodoacetic acid ( $\text{ICH}_2\text{COOH}$ , purchased from Sigma-Aldrich), as we reported in Ref. 24 of the main text. **Our previous measurement shows that the functionalization degree is ~ 25% -COOH per MoS<sub>2</sub>.**

Note that before membrane preparation, to remove possible ions contaminations, both the prepared MoS<sub>2</sub> solution and MoS<sub>2</sub>-COOH solution were washed with dilute trace-metal HCl (~2-5 mM), which was followed by filtration and redispersion in water under sonication (~10-15 min). The “HCl washing-filtration-redispersion” cycle was repeated at least three times. Then, the redispersed MoS<sub>2</sub> and MoS<sub>2</sub>-COOH solutions are dialyzed in dialysis tubings (Sigma-Aldrich, Part No. D9527-100FT) to remove extra HCl. Finally, repeated centrifugations (~4000 rpm/10min) were used to get the aqueous dispersion solutions of single- or few-layer MoS<sub>2</sub> and MoS<sub>2</sub>-COOH nanosheets (concentration 0.1-0.2 mg/ml), which were stored in HCl-washed plastic bottles and under 4 °C for use.

### **Preparation of MoS<sub>2</sub> membrane and MoS<sub>2</sub>-COOH membrane**

Both the MoS<sub>2</sub>-COOH membrane and MoS<sub>2</sub> membrane were prepared via the vacuum assisted filtration method. The substrate used is PTFE (pore size: 0.2 μm, purchased from Sigma-Aldrich, Part No. JGWP04700). Upon filtration, the MoS<sub>2</sub>/PTFE or MoS<sub>2</sub>-COOH/PTFE complex membranes were transferred to clean Petri dishes for natural air drying. To avoid membrane shrinkage or deformation, before membrane transfer, several drops of DI water were put beneath the complex membrane to remove air bubbles between PTFE and dishes. After the air-drying process, the prepared complex membranes were used for ion transport tests, membrane uptake tests and other characterizations, e.g. XAS, IR, XRD tests.

### **The IR tests**

The prepared MoS<sub>2</sub>-COOH membranes were transferred from the PTFE substrate to 1 mm thick CaF<sub>2</sub> substrates for IR absorption measurements. Prior to IR measurements, the membranes were soaked in individual salt solution (1M in D<sub>2</sub>O, D<sub>2</sub>O was purchased from Fisher Scientific, Part No. M1133660100) overnight to achieve ion uptake equilibrium, and were gently dried with tissue to remove the excess water immediately prior to the measurement. All spectra were measured in a Bruker Hyperion microscope coupled to a Bruker Vertex 70 FTIR spectrometer. The measurements were performed with a 0.4 NA Schwarzschild objective resulting in an IR focal spot of 100 μm diameter. Measurements were repeated to ensure the region of the sample was spatially uniform. Spectra were measured with a 2 cm<sup>-1</sup> resolution and 32 scans were averaged. The second derivative spectra were determined using a differentiating Savitzky-Golay filter.

### **XRD measurement**

The diffraction patterns in Bragg-Brentano geometry were obtained using a Rigaku benchtop Xray diffractometer equipped with HyPix-400 MF 2D hybrid pixel array detector (HPAD) and a Cu K $\alpha$  X-ray source (1.5406 Å) operating at 40 kV and 15 mA.

### **The membrane uptake tests**

The MoS<sub>2</sub>-COOH membranes or the MoS<sub>2</sub> membranes (typical mass loading 0.3-0.6 mg) were put into 3 ml solution of the mixed ions solutions or single salt solutions (K<sup>+</sup>, Mg<sup>2+</sup>, Cu<sup>2+</sup>, Cd<sup>2+</sup>, Pb<sup>2+</sup>) or binary salt solutions (Cu<sup>2+</sup>/Pb<sup>2+</sup>, K<sup>+</sup>/Pb<sup>2+</sup> and K<sup>+</sup>/Mg<sup>2+</sup>) or ternary salt solutions (K<sup>+</sup>/Mg<sup>2+</sup>/Pb<sup>2+</sup>) for at least overnight. Note that the pH or concentration of the solutions can be tuned. Then the membranes were taken out and thoroughly washed with flowing DI water (typically for ~ 2 min) to remove the mixed ions solution remaining on

the surface. Then the washed membranes were dissolved in 3ml HNO<sub>3</sub> (3%) under sonication overnight. Finally, the leaching HNO<sub>3</sub> solution was filtered and diluted for ICP-MS measurement. Ca<sup>2+</sup> uptake data are not included due to Mo interference in the ICP-MS test.

### **X-ray absorption spectroscopy (XAS) measurement**

XAS experiments were carried out at 20-ID-B,C, Advanced Photon Source of Argonne National Laboratory. Both Cu K-edge and Pb L3-edge XANES and EXAFS were measured under fluorescence mode by a Vortex ME4 detector. All XAS data analysis were performed with Athena software package to extract XANES and EXAFS. Fourier Transform of Cu and Pb EXAFS was performed by using Hanning window function with k-weights of 2 and k-range from 2 to 11 Å<sup>-1</sup>. For model-based EXAFS analysis, all the scattering paths were generated by the FEFF calculation function in Artemis based on the crystal structure of Cu(H<sub>2</sub>O)<sub>5</sub> and Pb(H<sub>2</sub>O)<sub>6</sub>. The generated scattering paths were then calibrated by performing the FEFF of the EXAFS data of those reference solution samples, mainly to obtain the amplitude reduction factor ( $S_0^2$ ) values. With  $S_0^2$  known, all EXAFS data of the membranes were fitted.

### **Scanning transmission electron microscopy measurement**

Scanning transmission electron microscopy experiments were carried out using aberration corrected JEOL ARM 200F with cold field emission gun. To minimize electron beam damage, the experiment was done at 80 kV which gives 1 Angstrom spatial resolution to allow single atom visualization.

## **Supplementary text**

### **The competitive permeation test of mixed ions across the membranes and calculations of effective diffusion coefficients**

A pair of H-cells was used for the competitive permeation test of mixed ions across the membranes, including the PTFE membrane, MoS<sub>2</sub>/PTFE complex membrane, MoS<sub>2</sub>-COOH/PTFE complex membrane and the commercial Nafion™ 117 membrane (thickness 0.007 inch, purchased from Sigma-Aldrich). These membranes were mounted in between the H-cells by commercial Silicon paste. The H-cells are ready for permeation tests after the solidification of the Silicon paste. Note that the Nafion membrane was activated in 3M H<sub>2</sub>SO<sub>4</sub> at 80 °C overnight followed by DI water rinsing for several times before use and the Nafion membrane was immersed in DI water environment during the solidification process of the Silicon paste.

In a competitive permeation test of mixed ions, 21 ml solution of mixed ions (~4 mM) and 21 ml deionized water were poured into the two chambers (the feed side and the permeate side) of H-cells simultaneously and respectively. Note that the MoS<sub>2</sub> or MoS<sub>2</sub>-COOH membrane faces the feed side. Both chambers were strongly stirred to avoid concentration polarization throughout the permeation tests. Then the concentration changes of every metal cation were monitored through periodic samplings (10-100µl per sampling subject to change according to permeation time), which were then diluted by 3% HNO<sub>3</sub> to 3-5 ml for ICP-MS measurements. Both chambers were tightly sealed with parafilm to avoid undesired evaporation throughout the process, except when sampling.

To perform quantitative analysis, we focus on the ion concentration changes in the permeate side at the very beginning, which take on linear increase versus time (**Figs. S5D**,

**6A, 7A, 10D, 11D 12A and 13A**). By calculating the slopes of linear profiles, we can get the permeation rates of all the ions,  $P_i$  (mol/s). The permeation rate of  $K^+$  ( $P_{K^+}$ ) is used as a reference, and is the largest among the cations studied.  $P_i$  values are plotted against the hydration radii and hydration enthalpies of the ions (**Table S1**), respectively, as shown in **Figs. S4 and 2A-C**. The effective diffusion coefficients of each ion across the membrane,  $D_{eff-i}$  ( $m^2/s$ ), can be further deduced according to the Fick's diffusion law reduced into one dimensional form:

$$P_i = - D_{eff-i} \Delta C_i S/d \quad (\text{Equation 1})$$

wherein  $\Delta C_i$  is the driving force, i.e. the concentration difference ( $mol/m^3$ ) between the permeate and the feed of the  $i$ th ion,  $S=\pi r^2$  is the area of the membrane ( $m^2$ ,  $r=0.75\text{ cm}$ ) and  $d$  is the thickness of the membrane (m).  $\Delta C_i$  can be approximated by the initial concentration in the feed,  $\Delta C_i \approx C_{i-feed, t=0}$ , given its small change at the very beginning. Also, we note here that even though level difference between the feed chamber and the permeate chamber can be always observed in the long-time test, the level difference was very small at the very beginning for a few hours and volume changes of both chambers were typically  $<2\%$ . We thus assumed that the volumes of both chambers are constant (21 ml) when applying Equation 1.

Considering the porosity ( $\phi$ ) and tortuosity ( $\tau$ ), the relationship between effective diffusion coefficient,  $D_{eff-i}$ , and ionic diffusion coefficient,  $D_{ion-i}$ , is

$$D_{eff-i} = \frac{\phi}{\tau} D_{ion-i} \quad (\text{Equation 2})$$

### Enhancement factor calculations

We calculate the enhancement factor (EF) of each cation, which is defined as the ratio of normalized ion permeation rate across the MoS<sub>2</sub>-based membranes to that across the PTFE membrane, i.e.

$$EF_i = \frac{P_i/P_K + (\text{membrane})}{P_i/P_K + (\text{PTFE})} \quad (\text{Equation 3})$$

The enhancement factor plots are shown in **Fig. S7** for the MoS<sub>2</sub>-COOH membrane and in **Fig. S6** for the MoS<sub>2</sub> membrane. Clearly, in the enhancement factor plots for both MoS<sub>2</sub>-based membranes: i) Cu<sup>2+</sup> and Pb<sup>2+</sup> are outliers and the enhancement factor of Pb<sup>2+</sup> in the MoS<sub>2</sub>-COOH membrane (up to 1.4) is the only case with value above 1; ii) The enhancement factor itself also shows a general decreasing trend versus the hydration radius and hydration enthalpy. The enhancement factor results also show the two distinct transport characteristics across the MoS<sub>2</sub>-based membrane discussed in the main text.

### **Kinetics of the ion transport across the MoS<sub>2</sub>-COOH membrane**

As a further attempt, we tried to determine the kinetics of the cations in the confined channels of MoS<sub>2</sub>-COOH membrane. Based on a simple transport picture, the permeation rate ( $P_i$ ) measured is the product of how many ions ( $C_{\text{memb}-i}$ , thermodynamics) and how fast the ions can move ( $V_i$ , kinetics) in the 2D confinement, as **Equation 4** shows

$$P_i \sim V_i C_{\text{memb}-i} \quad (\text{Equation 4})$$

wherein  $C_{\text{memb}-i}$  are the measured ion uptake concentrations in the membrane, while  $V_i$  characterizes the moving speeds of the cations in the membrane.

Using MoS<sub>2</sub>-COOH as an example with  $P_i$  (Fig. 2C) and  $C_{\text{memb-}i}$  (Fig. 3B) known, we can infer  $V_i$  according to Equation 4. As shown in **Fig. ST1**, in the MoS<sub>2</sub>-COOH membrane, Pb<sup>2+</sup> and Cu<sup>2+</sup> have moving speeds about one order of magnitude lower than the trivalent cations and about two to three orders of magnitude lower than the monovalent and other divalent cations. This result can be interpreted as showing that the strong interactions between Pb<sup>2+</sup>/Cu<sup>2+</sup> and the channel materials are equivalent to strong dragging forces prohibiting the ions from moving fast. Yet, the combined effects of thermodynamics and kinetics still give Pb<sup>2+</sup>/Cu<sup>2+</sup> enhanced permeation rate in the 2D confined channels. Thus we conclude in our original manuscript" ...we conclude that the anomalously enhanced transport of Pb<sup>2+</sup> and Cu<sup>2+</sup> arises from their strong interactions in the MoS<sub>2</sub>-based membranes over others, which thereby translate into huge thermodynamic advantages in their transport across the membrane."

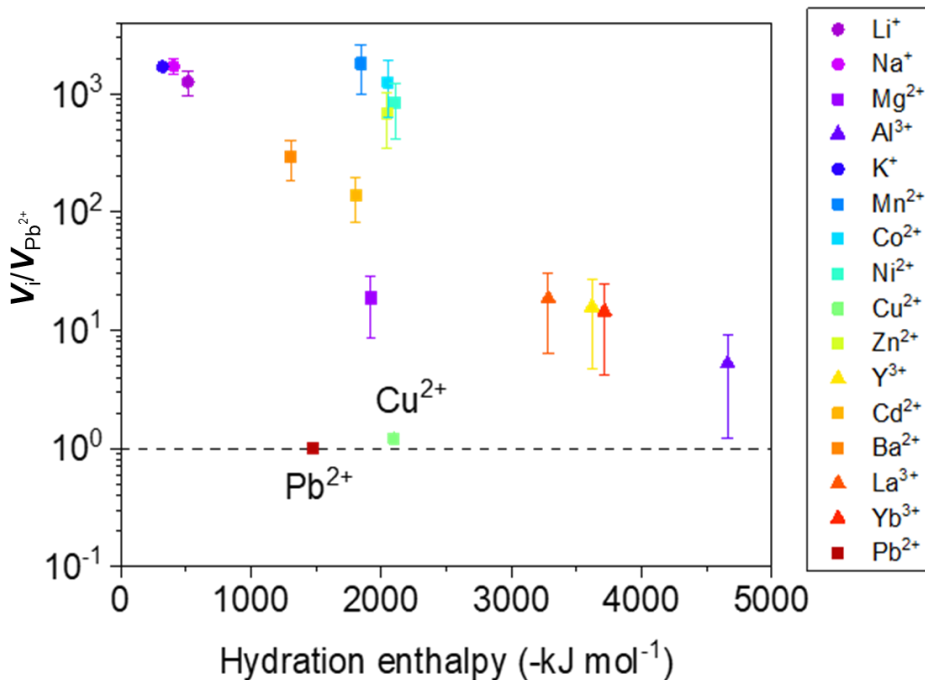


**Fig. ST1 The kinetics of cations transporting across the MoS<sub>2</sub>-COOH membrane.** The moving speed of the metal cations (relative to Pb<sup>2+</sup>) across the MoS<sub>2</sub>-COOH membrane versus the hydration enthalpies of the ions. Instead of K<sup>+</sup>, we chose Pb<sup>2+</sup> as the reference to compare the diffusion coefficients of the metal cations here, since the amount of Pb<sup>2+</sup> (Cu<sup>2+</sup>) uptake in the MoS<sub>2</sub>-COOH membrane can be reliably measured while K<sup>+</sup> cannot. We also note that even though the tiny to negligible uptake amounts for most of the cations in the ICP-MS test (typically ppb or even sub-ppb level measured) pose a challenge to obtaining accurate calculations here, the analysis is still semi-quantitatively revealing.

### **DFT calculations**

The MoS<sub>2</sub> monolayer (ML) is represented by a 4×4 supercell with 16 Mo atoms. The bilayer (BL) is formed by two parallel MLs with distances varying from 11-12 Å. One acetate group (-CH<sub>2</sub>COOH) is used to functionalize the ML and BL systems. The solvated divalent cation in bulk is represented by one cation and ten explicit H<sub>2</sub>O molecules. Two Cl<sup>-</sup> ions are used in each system to balance the charge. We have also employed a dielectric constant of  $\epsilon = 80.4$  to account for continuum solvation beyond the explicit waters. All the calculations are performed using the Vienna ab initio simulation package (VASP) based on spin-polarized density functional theory (DFT) with a plane-wave basis set and the projector-augmented wave (PAW)(32) technique. For geometry optimizations, the generalized gradient approximation (GGA) refined by Perdew, Burke, and Ernzerhof (PBE) (33) is utilized with Grimme's DFT-D3 correction (34) and BJ damping (35); and the energy- and force-convergence the parameters are  $1 \times 10^{-6}$  eV/cell and  $1 \times 10^{-2}$  eV/Å, respectively. The energy cutoff is 520 eV, and the Brillouin Zone is sampled using the  $\Gamma$ -

centered Monkhorst–Pack k-mesh of  $4\times4\times1$ . The  $\Gamma$  point ( $1\times1\times1$ ) is employed for cations in the bulk. The binding energy is defined as

$$E_{\text{BE}} = E_{\text{complex}} - (E_{\text{surface}} + E_{\text{bulk}}) \quad (\text{Equation 5})$$

where  $E_{\text{complex}}$ ,  $E_{\text{surface}}$ , and  $E_{\text{bulk}}$  denote the total energy of the complex, the surface energy (for ML or BL), and the energy of the cation in bulk, respectively. A void space of 12-15 Å above the slab is maintained in all structures.

DFT calculations provide insight into the binding of the metal ion with carboxylate-functionalized MoS<sub>2</sub>-COOH. We have performed a DFT study on Cu<sup>2+</sup> and Pb<sup>2+</sup> metal ions since they show the maximum uptake among all the metal ions in the mixture. We have also considered Zn<sup>2+</sup> since it is one of the metal ions which shows low uptake.

Cu<sup>2+</sup> in bulk is coordinated to five water molecules (**Fig. 5A**). For both ML and BL MoS<sub>2</sub>-COOH surface, Cu<sup>2+</sup> is coordinated to two water molecules, and one S of the surface. Monodentate coordination is observed between the O of the carboxylate group and Cu<sup>2+</sup> (**Fig. 5, B and C**). The monodentate coordination of Cu<sup>2+</sup> with the carboxylate group is also observed from the IR absorption spectra. Hence Cu<sup>2+</sup> sheds two water molecules, compared to the bulk, during the transport through the functionalized channel.

Hexa-coordination with water molecules is observed for Pb<sup>2+</sup> in bulk (**Fig. 5D**). In functionalized surfaces, bidentate coordination with the carboxylate group is observed for Pb<sup>2+</sup> for both ML and BL (**Figs. 5, E and F**). This agrees well with the IR absorption spectra results. Pb<sup>2+</sup> is coordinated to five water molecules in MoS<sub>2</sub>-COOH surfaces, indicating that it sheds one water molecule during the transport through the functionalized channel.

The binding energy increases in the bilayer channel compared to the monolayer surface for both Cu<sup>2+</sup> and Pb<sup>2+</sup>. The carboxylate group of MoS<sub>2</sub>-COOH surfaces are deprotonated in all the systems. Noteworthy in **Fig. 5B** is that the Cu-S distance is 2.13 Å, which is similar to the 2.05 Å distance associated with the CuS solid (36). This suggests that the Cu-S interaction may contribute a substantial fraction of the CuS bond energy (~3 eV) (37) to our calculated binding energy. This contrasts with Pb<sup>2+</sup>, which only shows negligible interaction with sulfur and the binding energy is more determined by the bidentate coordination with the acetate.

Note that we started our calculations with three different conformations, (i) monodentate binding to COO<sup>-</sup> (conf1) (ii) bidentate binding to COO<sup>-</sup> (conf2) and (iii) monodentate binding to COO<sup>-</sup> and simultaneously binding to S of MoS<sub>2</sub> surface (conf3). In case of Cu<sup>2+</sup> we found the conformer where Cu<sup>2+</sup> is binding to COO<sup>-</sup> in a monodentate fashion and also with S of MoS<sub>2</sub>. For Pb<sup>2+</sup> only the bidentate binding conformer was obtained.

Zn<sup>2+</sup> in bulk is coordinated to five water molecules (**Fig. S26**). For Zn<sup>2+</sup> we have considered only ML. We started our calculations with three different conformations, (i) monodentate binding to COO<sup>-</sup> (conf 1) (ii) bidentate binding to COO<sup>-</sup> (conf 2) and (iii) monodentate binding to COO<sup>-</sup> and simultaneously binding to S of MoS<sub>2</sub> surface (conf 3). We could isolate conf1 and conf3 for Zn<sup>2+</sup>. Conf1 is stable than conf3 by 0.18 eV. The binding energies are -0.68 eV for conf1 and -0.50 eV for conf3. The structures are represented in **Figure S26**. This result indicates that Zn<sup>2+</sup> binds more weakly than Cu<sup>2+</sup> or Pb<sup>2+</sup> (Fig. 5) which is consistent with the smaller uptake for Zn<sup>2+</sup>.

The model used in DFT calculations with 10 explicit water molecules is an approximate model, suitable for binding mode analysis associated with changes in the first coordination

sphere. Determination of the bilayer spacing ( $d$ ) requires the inclusion of more explicit water molecules and is beyond the scope of this study.

### **Dynamic membrane uptake test**

The MoS<sub>2</sub>-COOH membrane (0.69 mg) on the PTFE substrate was put into a 3 ml mixture solution (~ 0.45 mM, Cl<sup>-</sup>/NO<sub>3</sub><sup>-</sup>≈96:44). Periodic samplings of the solution were made to monitor the ion concentration change in the solution. The sampled solutions were diluted by 3% HNO<sub>3</sub> for ICPMS measurements. The solution was strongly stirred throughout the test. All tests were done at room temperature. The results are shown as **Fig. S25**.

### **High-Energy X-ray Scattering with Pair Distribution Function (HEXS-PDF) Analysis.**

Experiment: The total X-ray scattering measurements were carried out at the Advanced Photon Source (APS, beamline 11-ID-B), using a high energy of 58.6 keV, which corresponds to an X-ray wavelength of 0.2116 Å. During the measurements, the MoS<sub>2</sub>-based membranes were placed between two pieces of Kapton ® Tapes, and then put on the X-ray pathway with a sample-to-detector distance of 180 mm which was further calibrated using CeO<sub>2</sub> (SRM 674b) as the standard material. For each sample, a total of 11 scattering images were collected, where each scattering image was obtained using 1000 0.3-s exposures (*i.e.*, 5-min collection time in total). Following the X-ray scattering measurements, each scattering image was integrated into reciprocal-space diffraction patterns using the GSAS-II (38), from which an average diffraction pattern was calculated for each sample by averaging the diffraction patterns derived from the 11 scattering images. Finally, PDFgetX3 was used to convert the diffraction patterns to real-space PDF (39).

**Results and Discussions:** To get additional insights into the effects of ions on the atomic structures of MoS<sub>2</sub> and MoS<sub>2</sub>-COOH, high-energy X-ray scattering experiments were carried out and data were then processed using the pair distribution function analysis (**Figure S17**). For comparison, the PDF of a MoS<sub>2</sub> model, which was obtained from the crystallography open database (Entry 9007660 (40)), was first calculated using DiffPy-CMI (41) and plotted in **Figure S17A** along with the partial PDFs. More specifically, the PDF of the MoS<sub>2</sub> model contains both local, intermediate, and long-range atomic distances, which originated from the Mo-Mo, Mo-S, and S-S correlations. Some characteristic intralayer atomic correlations (**Figure S17, B and E**) were observed from the PDF of the MoS<sub>2</sub> model, such as the 1<sup>st</sup> shell Mo-S correlation (2.38 Å), 2<sup>nd</sup> shell Mo-Mo correlation (3.16 Å), 2<sup>nd</sup> shell S-S correlation (3.16 Å), and 3<sup>rd</sup> shell Mo-S correlation (3.94 Å and 5.06 Å). In addition to the intralayer atomic correlations, interlayer atomic correlations were also observed, including but not limited to the interlayer Mo-S and Mo-Mo correlations at 5.62 Å and 6.38 Å, respectively (**Figure S17B**). In comparison, the experimental results (**Figures S17, C and D**) of our prepared samples all share similar atomic distances with the MoS<sub>2</sub> model regarding the first three coordination shells, except for one additional atomic correlation at ~2.75 Å predominately shown on the experimental data, which could be attributed to the additional Mo-Mo correlation caused by structural deformation of MoS<sub>2</sub>.(42, 43) Despite the similarity in atomic distances in the local structures of MoS<sub>2</sub> and MoS<sub>2</sub>-COOH samples, slight differences were observed in the weights of the local atomic correlations. For example, the PDFs of the MoS<sub>2</sub>-COOH samples exhibit stronger contributions from the first two atomic correlations and weaker atomic correlations at ~3.16 Å when compared with the MoS<sub>2</sub> samples, which might stem from the additional

atomic correlations associated with the acetate groups after the functionalization of MoS<sub>2</sub>. Moreover, the functionalization of MoS<sub>2</sub> with acetate groups also increased the interlayer spacing as evidenced by the increased interlayer Mo-Mo distance (6.63 Å) in MoS<sub>2</sub>-COOH compared with 6.34 Å in the pristine MoS<sub>2</sub> sample (**Figure S17E**). In terms of ion modifications, Cu and Pb showed a significant effect on the interlayer spacing of MoS<sub>2</sub> by increasing the interlayer Mo-Mo distance by 0.23 Å and 0.34 Å, respectively. In contrast, minimal changes ( $\leq 0.03$  Å) were observed in the interlayer Mo-Mo distance of the MoS<sub>2</sub>-COOH after the Cu and Pb modifications (**Figure S17E**), suggesting negligible structural modifications.

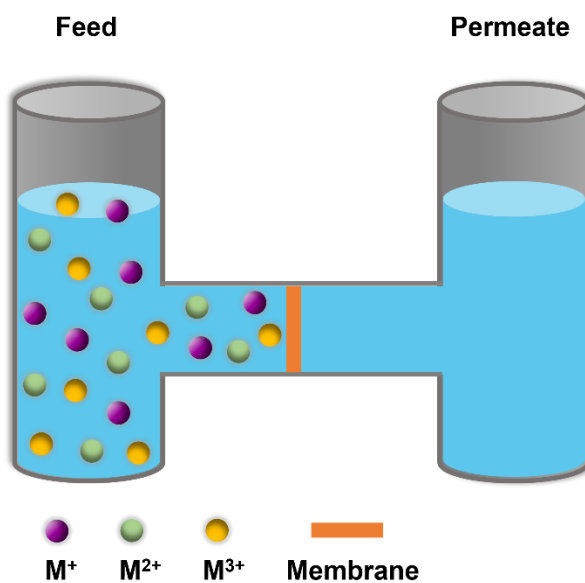


**Fig. S1 Schematic of the competitive permeation test of mixed ions using an H-type cell.** One chamber is the feed, i.e. a mixture solution of seventeen kinds of metal cations. The other chamber is the permeate, i.e. deionized water of the same volume. The membranes to be tested were mounted in between the two chambers. The membranes can

be bare commercial hydrophilic PTFE (pore size ~ 200 nm), MoS<sub>2</sub>/PTFE and MoS<sub>2</sub>-COOH/PTFE complex membranes or the commercial Nafion™ 117 membrane. Both chambers are strongly stirred to mitigate concentration polarizations.

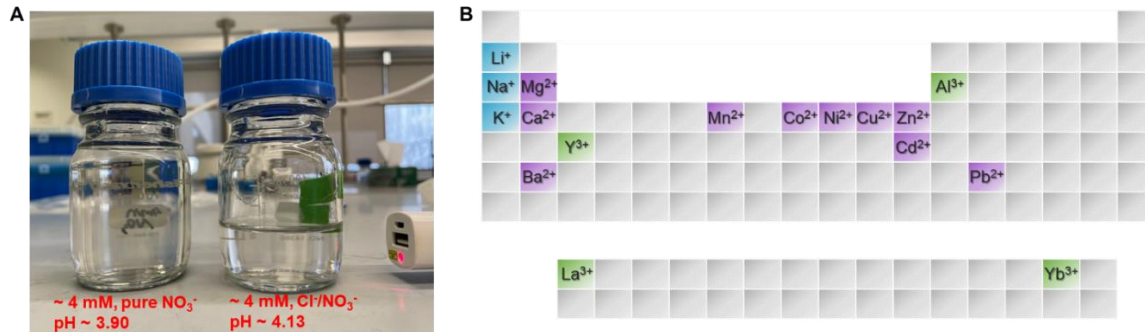


**Fig. S2 Mixed ions solutions.** (A) The photo of mixed ions solutions. One has pure  $\text{NO}_3^-$  anions ( $\sim 4\text{mM}$  of each cation,  $\text{pH}\sim 3.90$ ) and the other has dominant  $\text{Cl}^-$  anions ( $\sim 4\text{mM}$  of each cation,  $\text{Cl}^-/\text{NO}_3^- \approx 96 \text{ mM}:44 \text{ mM}$ ,  $\text{pH}\sim 4.13$ ). Both are clear and stable solutions without colloidalization or precipitation. No Tyndall effect was observed. (B) The distribution of the selected cations in the periodic table.

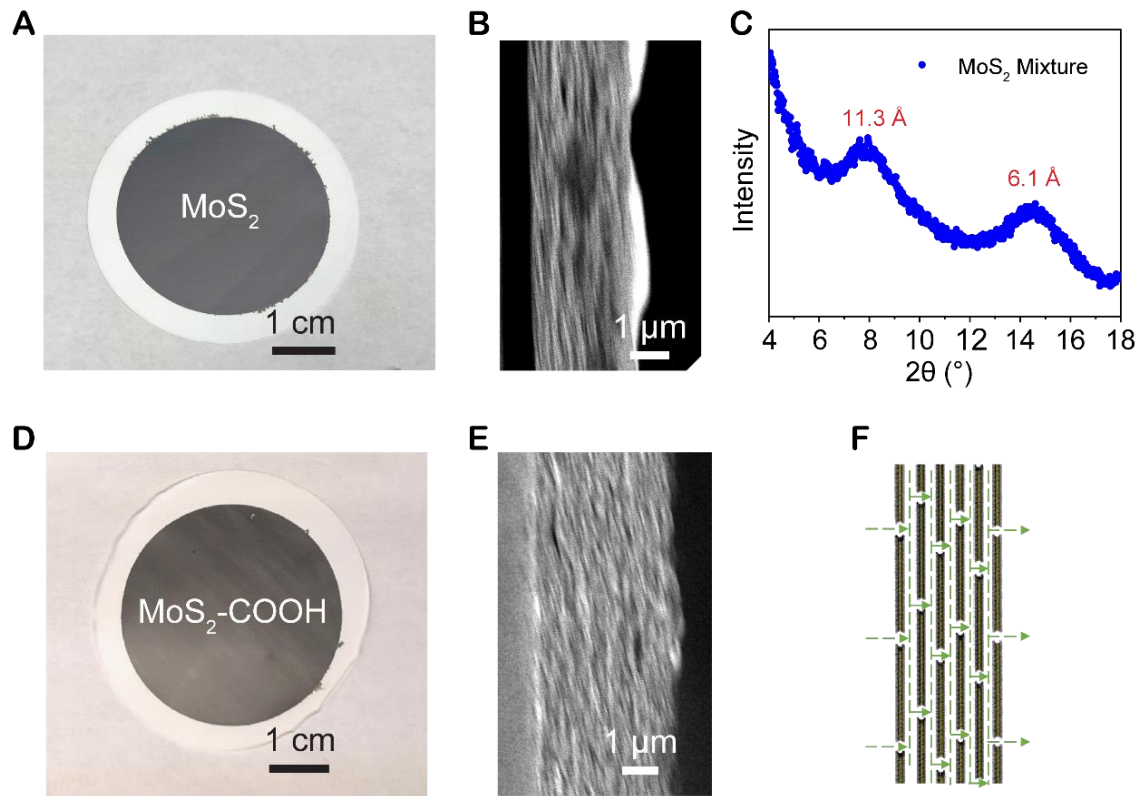


**Fig. S3 MoS<sub>2</sub> based membranes.** (A) Photo of the restacked MoS<sub>2</sub> membranes on PTFE substrate. (B) Cross-sectional SEM image of the restacked MoS<sub>2</sub> membranes. (C) Representative XRD spectrum of MoS<sub>2</sub> membrane in the mixture solution (anions: Cl<sup>-</sup>/NO<sub>3</sub><sup>-</sup>). The peak  $\sim 14.4^{\circ}$  ( $\sim 6.1 \text{ \AA}$ ) corresponds to the bulk MoS<sub>2</sub>, suggesting the blocked channels due to irreversible dehydration/hydration of pristine MoS<sub>2</sub> membrane. (D) Photo of the restacked MoS<sub>2</sub>-COOH membranes on PTFE substrate. (E) Cross-sectional SEM image of the restacked MoS<sub>2</sub>-COOH membranes. (F) Schematic illustration of the ion pathways within the restacked membranes.

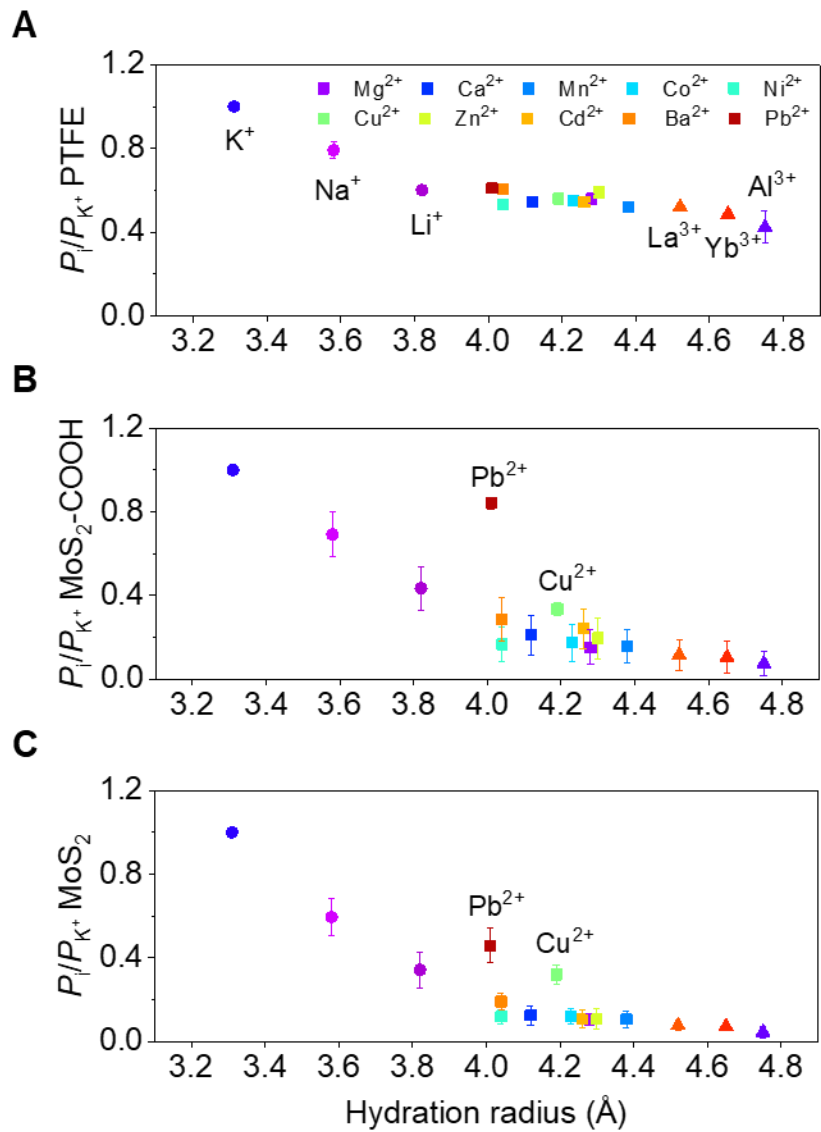


**Fig. S4 Ion transport across the membranes.** (A, B, C) The ion permeation rates versus the hydration radius of the ions across the PTFE membrane, MoS<sub>2</sub>-COOH membrane and MoS<sub>2</sub> membrane, respectively. Feed: ~ 4 mM, Cl<sup>-</sup>/NO<sub>3</sub><sup>-</sup> anions, pH ~ 4.13.

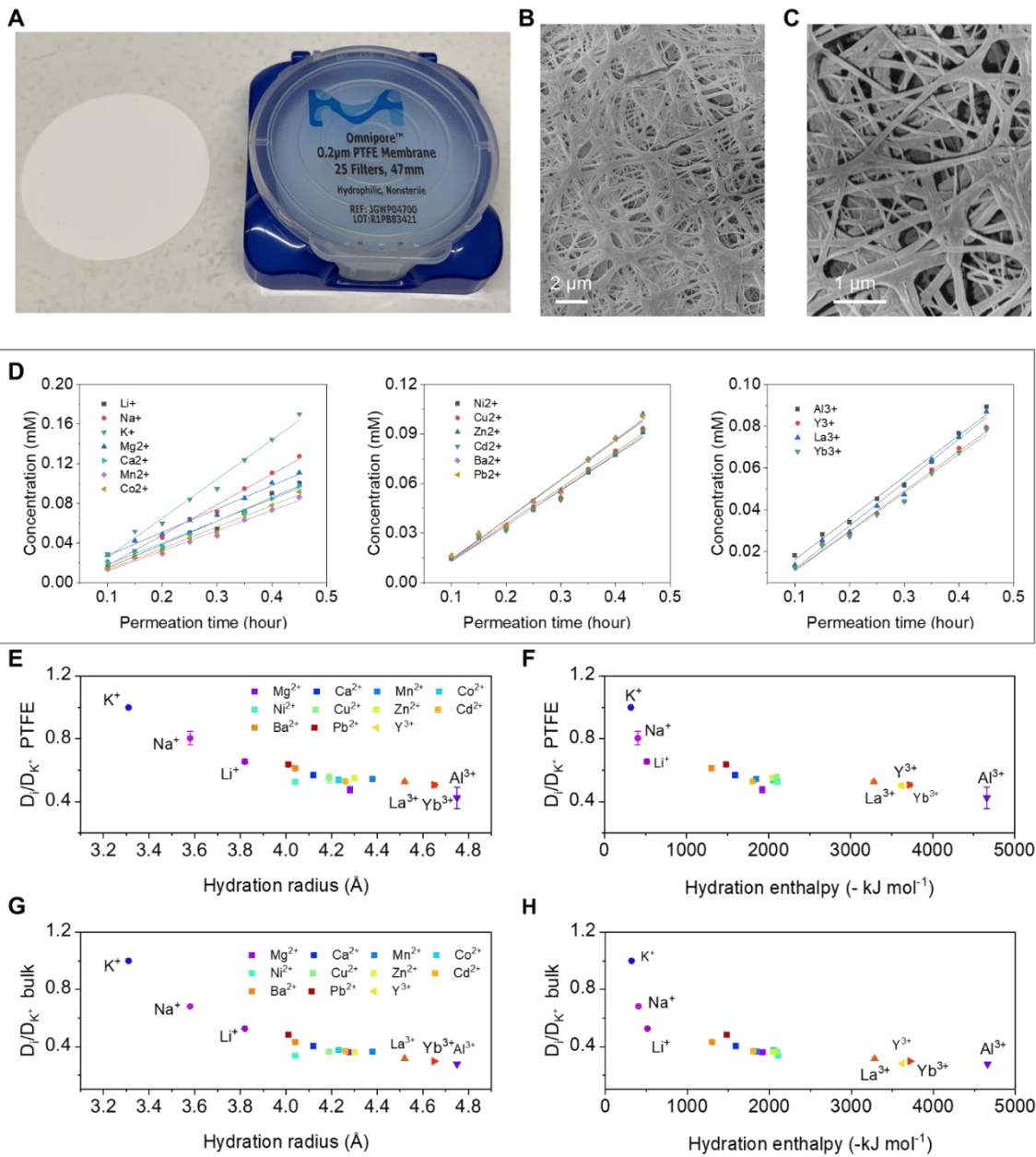


**Fig. S5 Ion transport across the PTFE membrane.** (A) Photo of the commercial PTFE membrane used. (B, C) SEM images of the PTFE membrane showing the pores. 5 nm Pd/Pt were coated to eliminate the charging effect during imaging. (D) The concentration profiles of all metal cations in the permeate side across the hydrophilic PTFE membrane (pore size  $\sim 200$  nm and thickness  $\sim 65$   $\mu\text{m}$ ). (E, F) The *effective* diffusion coefficients of the metal cations (relative to  $\text{K}^+$ ) across the PTFE membrane versus the hydration radii and hydration enthalpies of the ions, respectively.  $D_{\text{eff-K}^+-\text{PTFE}} \approx 2.331 \times 10^{-10} \text{ m}^2/\text{s}$ . Feed solution:  $\sim 4\text{mM}$ ,  $\text{Cl}^-/\text{NO}_3^-$ ,  $\text{pH} \sim 4.13$ . (G, H) The bulk diffusion coefficients of the metal cations versus the hydration radii and hydration enthalpies of the ions, respectively. The tabulated bulk diffusion coefficients of the metal cations in D and E are from Ref. (44) and

listed in **Table S1**, where  $D_{K^+ \text{-bulk}} = 1.957 \times 10^{-9} \text{ m}^2/\text{s}$ . The difference between the  $D_{\text{eff-K}^+ \text{-PTFE}}$  and  $D_{K^+ \text{-bulk}}$  can be attributed to the porosity and tortuosity of the PTFE membrane, as **Equation 2** suggests.

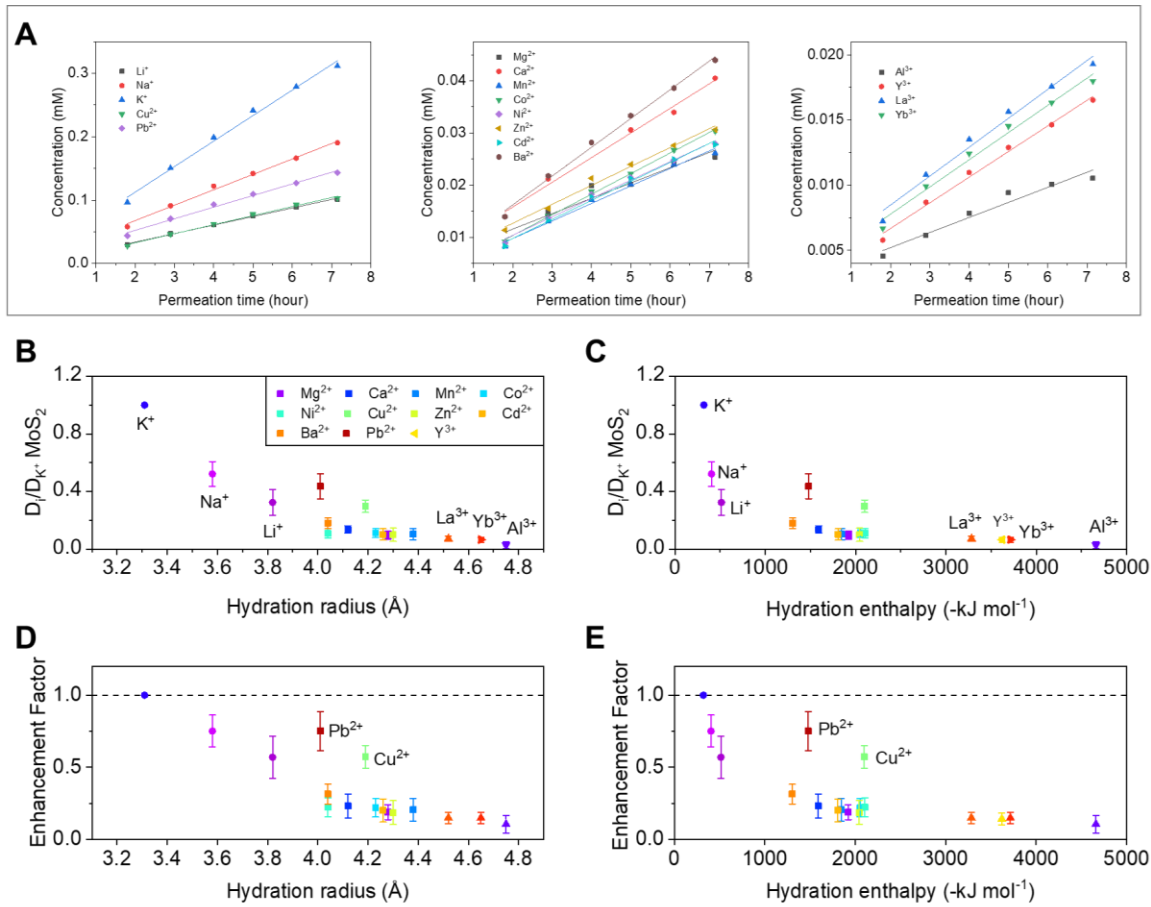


**Fig. S6 Ion transport across the MoS<sub>2</sub> membrane.** (A) The typical concentration profiles of all metal cations in the permeate side across the MoS<sub>2</sub> membrane. (B, C) The *effective* diffusion coefficients of the metal cations (relative to K<sup>+</sup>) across the MoS<sub>2</sub> membrane versus the hydration radii and hydration enthalpies of the ions, respectively.  $D_{\text{eff-}K^+\text{-MoS}_2}$  is  $\sim 3.31 \times 10^{-14} \text{ m}^2/\text{s}$ . (D, E) The enhancement factor across the MoS<sub>2</sub> membrane versus the hydration radii and hydration enthalpies of the ions, respectively. The error bars come from independent tests of three MoS<sub>2</sub> membranes. Feed solution:  $\sim 4 \text{ mM Cl}^-/\text{NO}_3^-$ , pH  $\sim 4.13$ . Note that the measured ion permeation rates of the MoS<sub>2</sub> membranes are much smaller than that of the bare PTFE membrane substrate. So the measured ion permeation rates and other parameters deduced essentially reflect their transport properties across the MoS<sub>2</sub> membrane, even though MoS<sub>2</sub>/PTFE complex membrane was used in the permeation test.

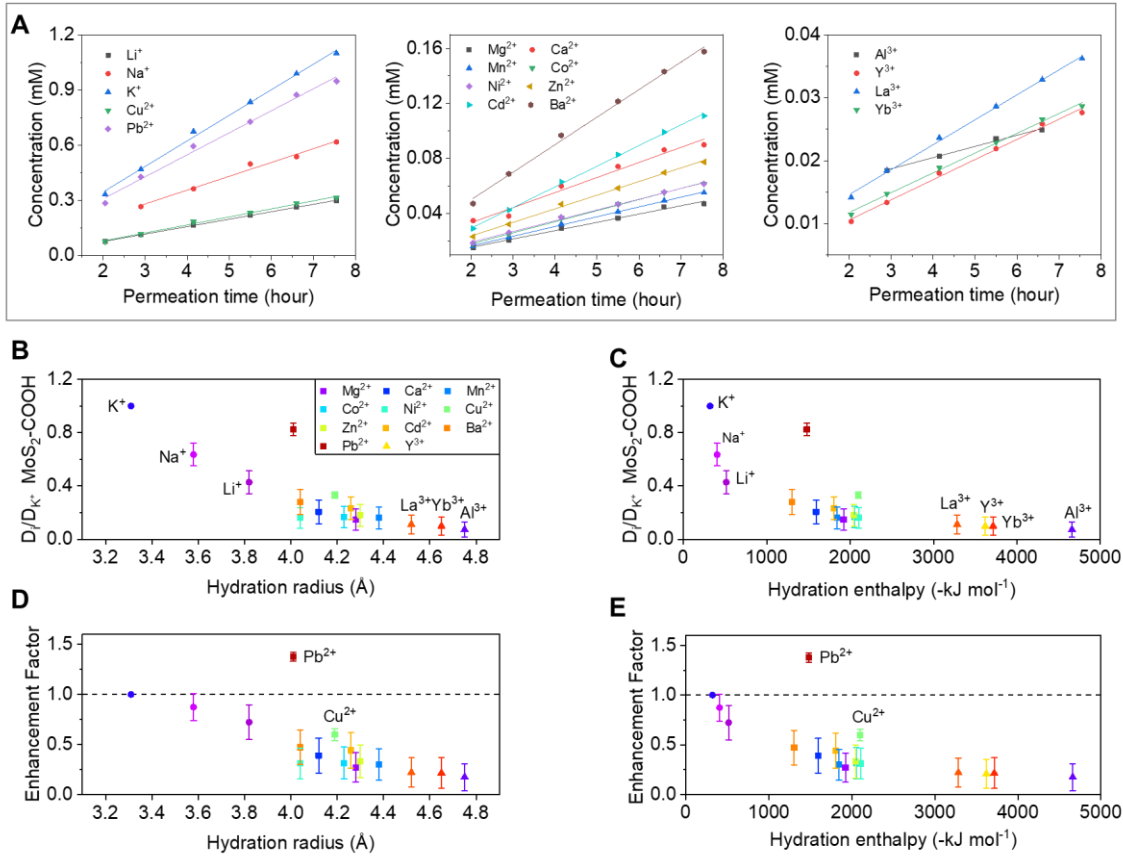


**Fig. S7 Ion transport across the  $\text{MoS}_2\text{-COOH}$  membrane.** (A) The typical concentration profiles of all metal cations in the permeate side across the  $\text{MoS}_2\text{-COOH}$  membrane. (B, C) The *effective* diffusion coefficients of the metal cations (relative to  $\text{K}^+$ ) across the  $\text{MoS}_2\text{-COOH}$  membrane versus the hydration radii and hydration enthalpies of the ions, respectively.  $D_{\text{eff}, \text{K}^+ \text{-MoS}_2\text{-COOH}} \sim 2.229 \times 10^{-13} \text{ m}^2/\text{s}$ . (D, E) The enhancement factor across the  $\text{MoS}_2\text{-COOH}$  membrane versus the hydration radii and hydration enthalpies of the ions, respectively. The error bars come from independent tests of three  $\text{MoS}_2\text{-COOH}$  membranes. Feed solution:  $\sim 4 \text{ mM}$ ,  $\text{Cl}^-/\text{NO}_3^-$ ,  $\text{pH} \sim 4.13$ . Note that the measured ion permeation rates of the  $\text{MoS}_2\text{-COOH}$  membranes are much smaller than that of the bare PTFE membrane substrate. So the measured ion permeation rates and other parameters deduced essentially reflect their transport properties across the  $\text{MoS}_2\text{-COOH}$  membrane, even though  $\text{MoS}_2\text{-COOH/PTFE}$  complex membrane was used in the permeation test.

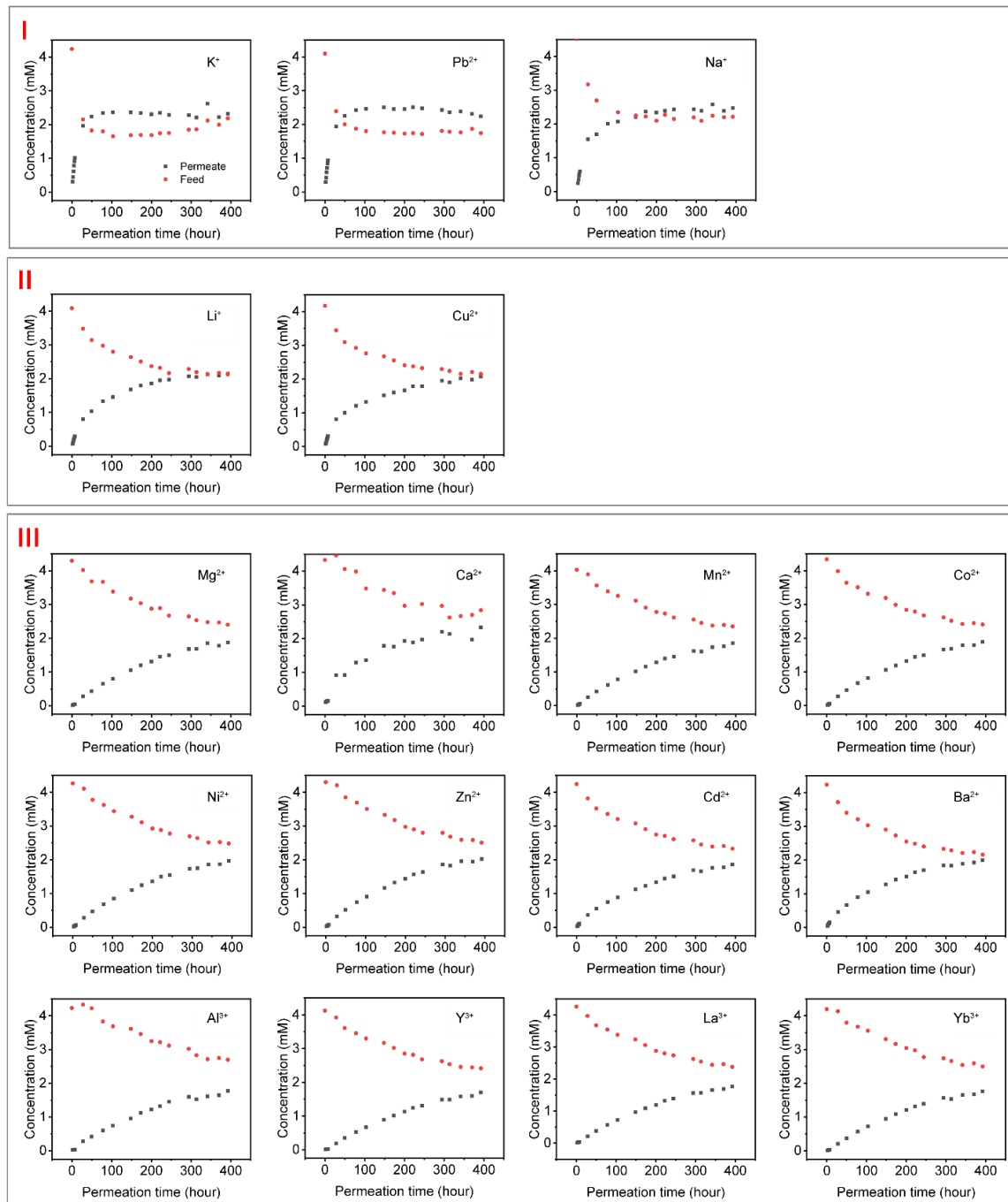


**Fig. S8 The concentration profiles of all metal cations across the MoS<sub>2</sub>-COOH membrane.** The concentration profiles are categorized into three types, according to the profile shapes. Cations of type I have a concentration crossover between the feed and the permeate, while type II and type III show concentration equilibria and nonequilibria between the feed and the permeate, respectively. Feed solution: ~ 4mM, Cl<sup>-</sup>/NO<sub>3</sub><sup>-</sup>, pH ~ 4.13.

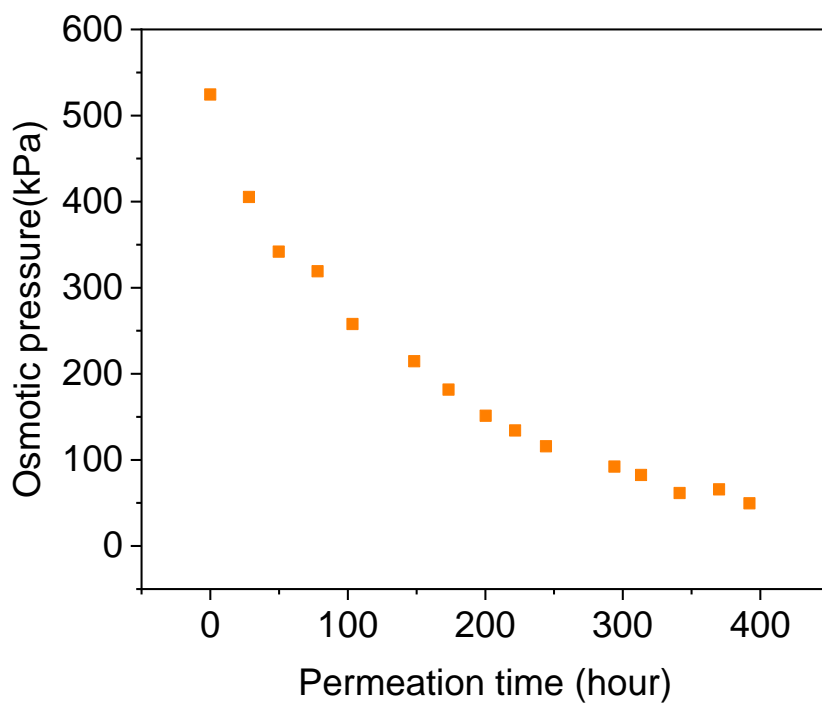


**Fig. S9** The evolution of the osmotic pressure across the MoS<sub>2</sub>-COOH membrane test corresponding to Fig. S8.

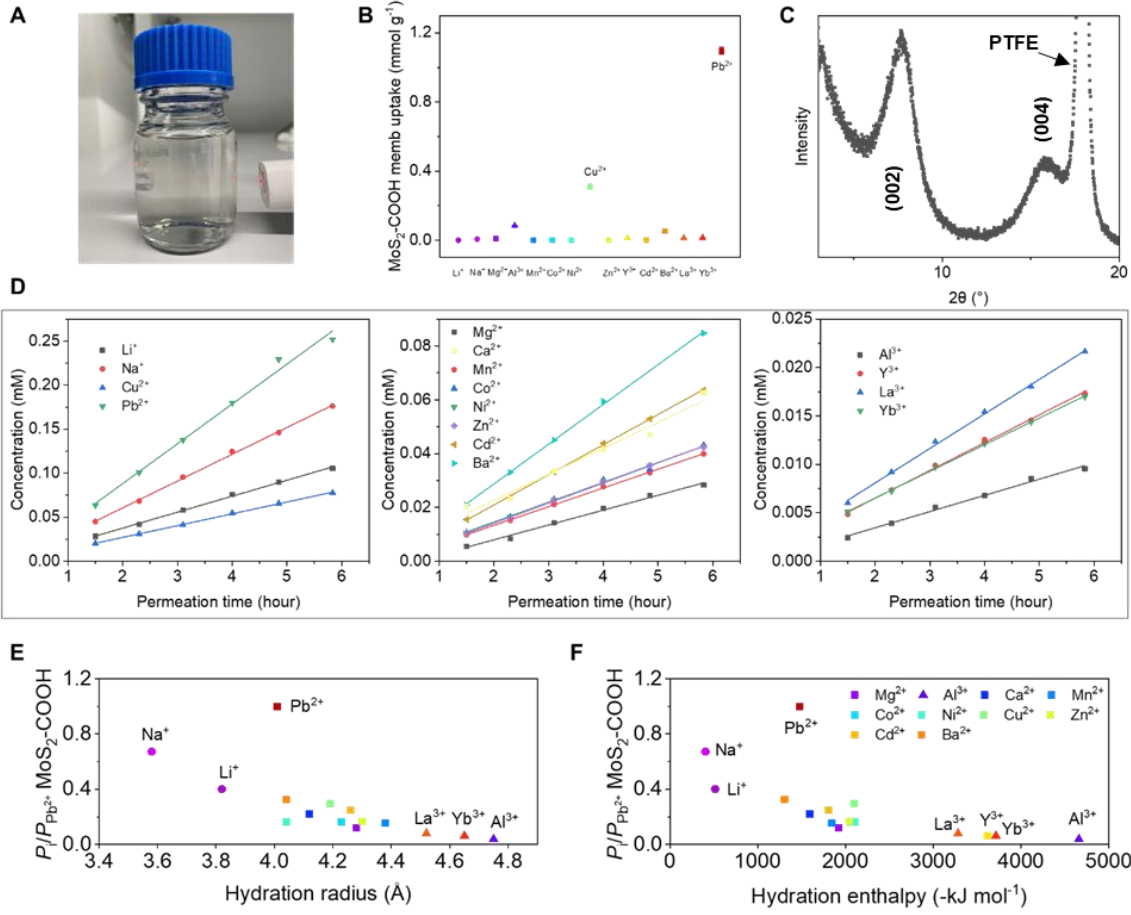


**Fig. S10 Tests of mixed ion without K<sup>+</sup>.** (A) Photo of the mixed ion solution without K<sup>+</sup>. To maintain the same total ionic strength of the mixture, the concentration of all the cations is tuned to be ~ 4.07 mM. Mixture: pH ~ 4.02; molar ratio Cl<sup>-</sup>:NO<sub>3</sub><sup>-</sup>=23:11. (B) The uptake of MoS<sub>2</sub>-COOH membrane in the mixed ion solution without K<sup>+</sup>, showing preponderant uptake of Cu<sup>2+</sup> and Pb<sup>2+</sup>. (C) The XRD spectrum of MoS<sub>2</sub>-COOH membrane in the mixed ion solution without K<sup>+</sup>. This interlayer spacing is ~ 11.4 Å, same as the one in the mixed ion solution with K<sup>+</sup> (**Fig. 1D**). D-F correspond to the ion transport results across the MoS<sub>2</sub>-COOH membrane using the mixed ions solution without K<sup>+</sup>. (D) The concentration profiles of all mixed metal cations (without K<sup>+</sup>) in the permeate side across the MoS<sub>2</sub>-COOH membrane. (E, F) The ion permeation rates of the metal cations (relative to Pb<sup>2+</sup>) across the MoS<sub>2</sub>-COOH membrane versus the hydration radii and hydration enthalpies of the ions, respectively.

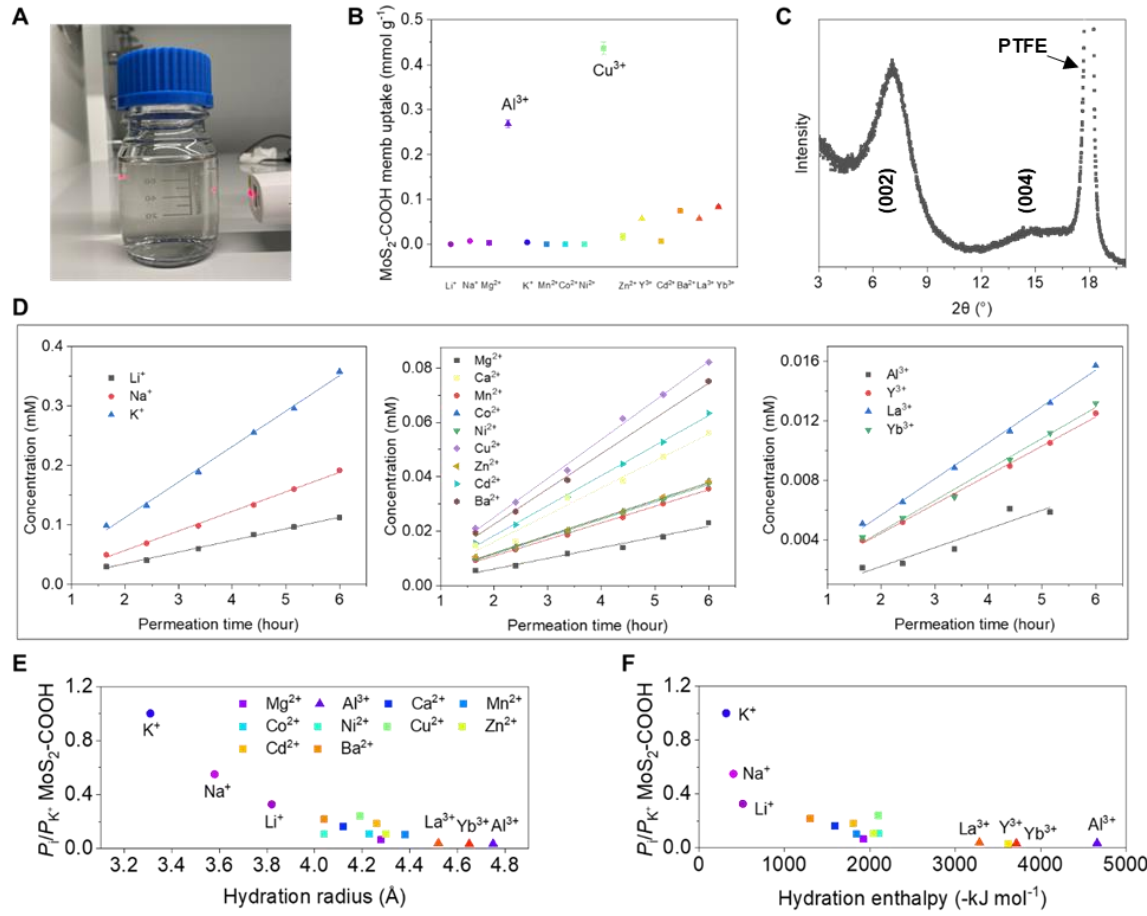


**Fig. S11 Tests of mixed ion without  $\text{Pb}^{2+}$ .** (A) Photo of the mixed ion solution without  $\text{Pb}^{2+}$ . To maintain the same total ionic strength of the mixture, the concentration of all the cations is tuned to be  $\sim 4.22 \text{ mM}$ . Mixture: pH  $\sim 4.00$ ; molar ratio  $\text{Cl}^-:\text{NO}_3^- = 24:9$ . (B) The uptake of  $\text{MoS}_2\text{-COOH}$  membrane in the mixed ion solution without  $\text{Pb}^{2+}$ , showing preponderant uptake of  $\text{Cu}^{2+}$  and  $\text{Al}^{3+}$ . (C) The XRD spectrum of  $\text{MoS}_2\text{-COOH}$  membrane in the mixed ion solution without  $\text{Pb}^{2+}$ . This interlayer spacing is  $\sim 12.5 \text{ \AA}$ , closer to the value of  $\text{Al}^{3+}$  treated  $\text{MoS}_2\text{-COOH}$  membrane ( $\sim 12.6 \text{ \AA}$ ) rather than that of  $\text{Cu}^{2+}$  treated one ( $\sim 11.9 \text{ \AA}$ , Table S2). (D-F) correspond to the transport results of the mixed ions solution without  $\text{Pb}^{2+}$  across the  $\text{MoS}_2\text{-COOH}$  membrane. (D) The concentration profiles of all mixed metal cations (without  $\text{Pb}^{2+}$ ) in the permeate side across the  $\text{MoS}_2\text{-COOH}$  membrane. (E, F) The ion permeation rates of the metal cations (relative to  $\text{K}^+$ ) across the  $\text{MoS}_2\text{-COOH}$  membrane versus the hydration radii and hydration enthalpies of the ions, respectively.

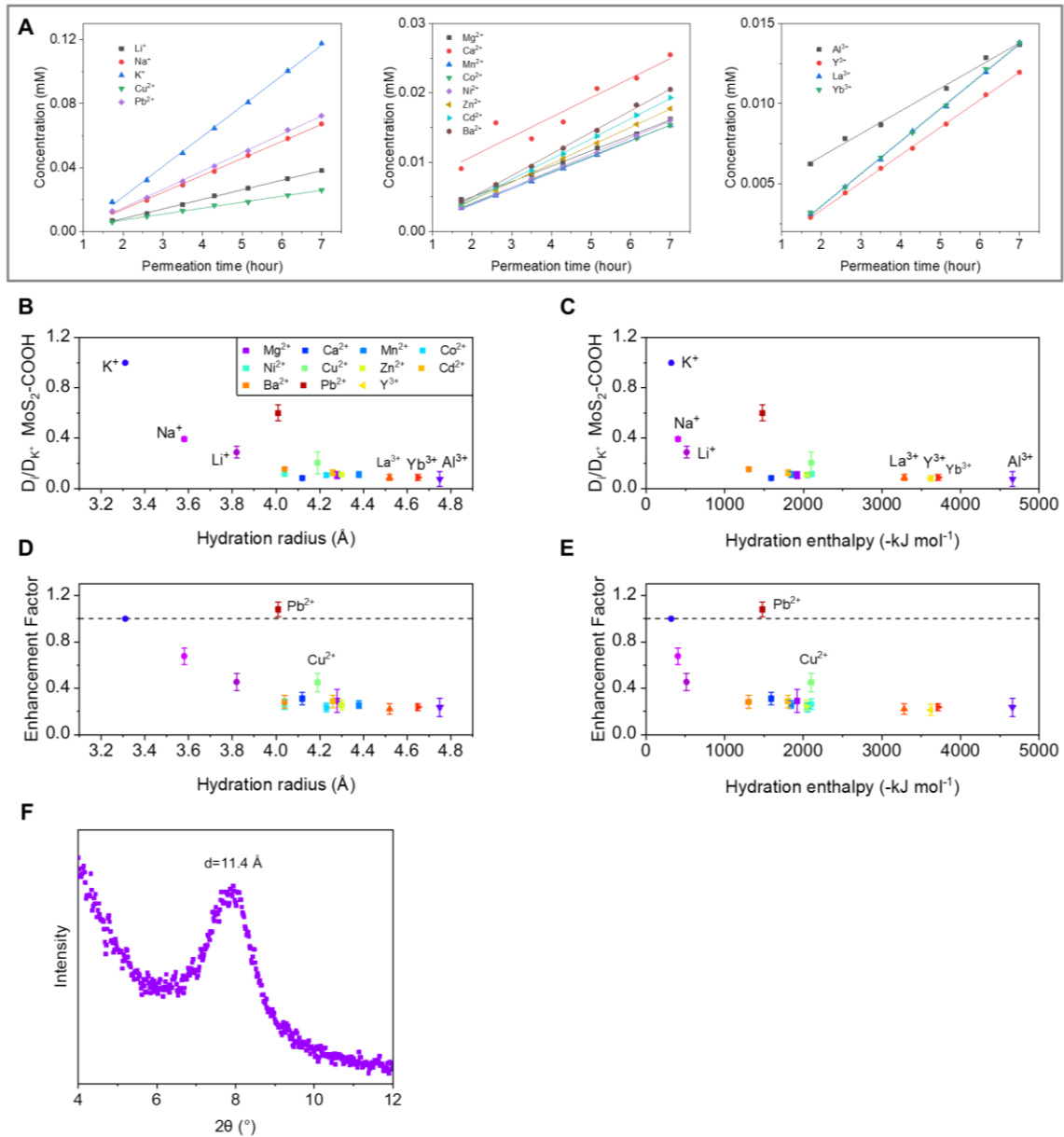


**Fig. S12 The anion effect.** (A) The typical concentration profiles of all metal cations in the permeate side across the  $\text{MoS}_2\text{-COOH}$  membrane. Feed solution:  $\sim 4\text{mM}$ , pure  $\text{NO}_3^-$ , pH  $\sim 3.90$ .

(B, C) The *effective* diffusion coefficients of the metal cations (relative to  $\text{K}^+$ ) across the  $\text{MoS}_2\text{-COOH}$  membrane versus the hydration radii and hydration enthalpies of the ions, respectively. (D, E) The enhancement factor of the ion transport across the  $\text{MoS}_2\text{-COOH}$  membrane versus the hydration radii and hydration enthalpies of the ions, respectively. (F) The XRD spectrum of  $\text{MoS}_2\text{-COOH}$  membrane in the mixture with pure nitrate anions.

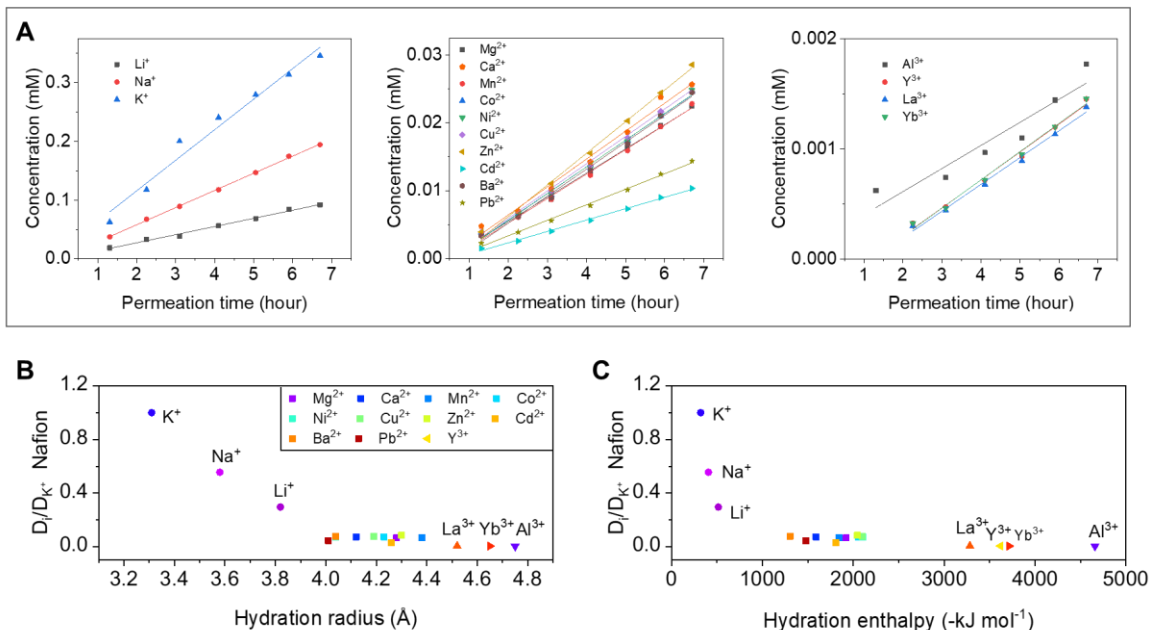


**Fig. S13 Ion transport across the Nafion™ 117 membrane.** (A) The concentration changes of all metal cations in the permeate side across the Nafion™ 117 membrane. (B, C) The *effective* diffusion coefficients of the metal cations (relative to  $\text{K}^+$ ) across the Nafion™ 117 membrane versus the hydration radii and hydration enthalpies of the ions, respectively. Feed solution:  $\sim 4 \text{ mM, Cl}^-/\text{NO}_3^-$ , pH  $\sim 4.13$ .  $D_{\text{eff-K}^+\text{-Nafion}}$  is  $\sim 7.785 \times 10^{-11} \text{ m}^2/\text{s}$ . The measured  $D_{\text{eff-K}^+\text{-Nafion}}$  is comparable with the reported values Ref. (45).

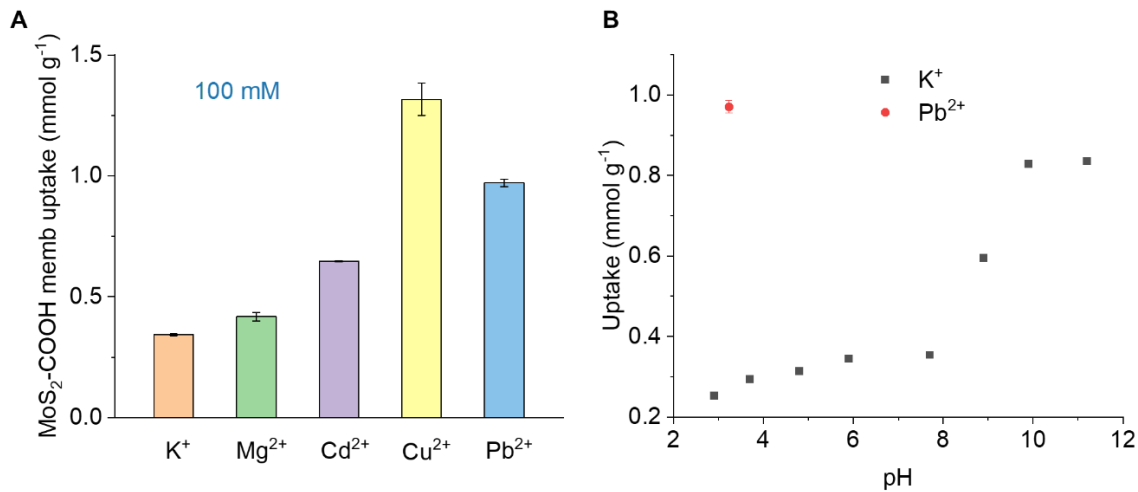


**Fig. S14 (A)** The uptake of  $\text{MoS}_2\text{-COOH}$  membrane in single metal cation solution (~100 mM). pH values: 100 mM  $\text{KNO}_3 \sim 5.60$ /4 mM  $\text{KNO}_3 \sim 6.45$ ; 100 mM  $\text{Mg}(\text{NO}_3)_2 \sim 5.64$ /4 mM  $\text{Mg}(\text{NO}_3)_2 \sim 5.50$ ; 100 mM  $\text{Cd}(\text{NO}_3)_2 \sim 4.89$ ; 100 mM  $\text{Cu}(\text{NO}_3)_2 \sim 3.93$ /4 mM  $\text{Cu}(\text{NO}_3)_2 \sim 4.63$ ; 100 mM  $\text{Pb}(\text{NO}_3)_2 \sim 3.23$ /4 mM  $\text{Pb}(\text{NO}_3)_2 \sim 4.27$ . **(B)** The pH-dependent uptake of  $\text{K}^+$  (100 mM) in the  $\text{MoS}_2\text{-COOH}$  membrane. The  $\text{Pb}^{2+}$  data point in (B) is taken from (A). All the pH values in (B) are the nominal ones of the starting solution, and we observed a reduction of all solutions' pH after uptake due to the deprotonation of the -COOH.

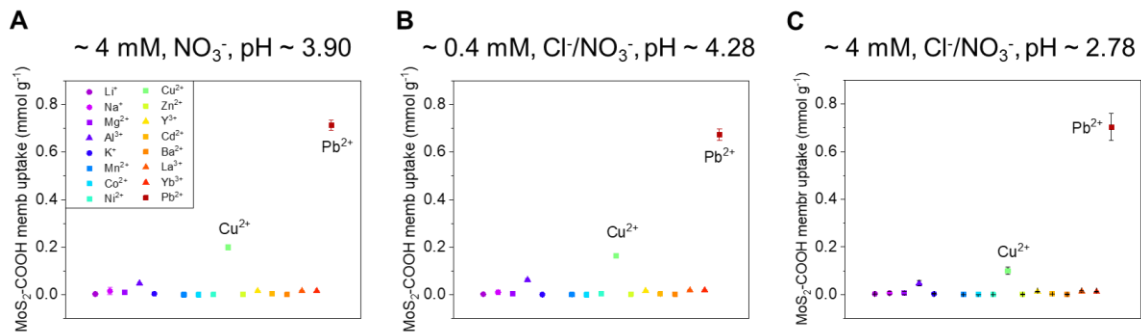


**Fig. S15 The anion effect, concentration effect and pH effect on the uptake of the metal cations in the  $\text{MoS}_2\text{-COOH}$  membrane.** (A) Uptake condition: ~ 4 mM, pure  $\text{NO}_3^-$ , pH ~ 3.90. (B) Uptake condition: ~ 0.4 mM,  $\text{Cl}^-/\text{NO}_3^-$ , pH ~ 4.28. (C) Uptake condition: ~ 4 mM,  $\text{Cl}^-/\text{NO}_3^-$ , pH ~ 2.78. The pH in (B) is the natural pH after diluting the parent solution (~ 4 mM,  $\text{Cl}^-/\text{NO}_3^-$ , pH ~ 4.13). The pH in (C) was tuned by adding high-purity concentrated  $\text{HNO}_3$  into the parent solution (~ 4 mM,  $\text{Cl}^-/\text{NO}_3^-$ , pH ~ 4.13). The volume change with  $\text{HNO}_3$  adding was negligible.

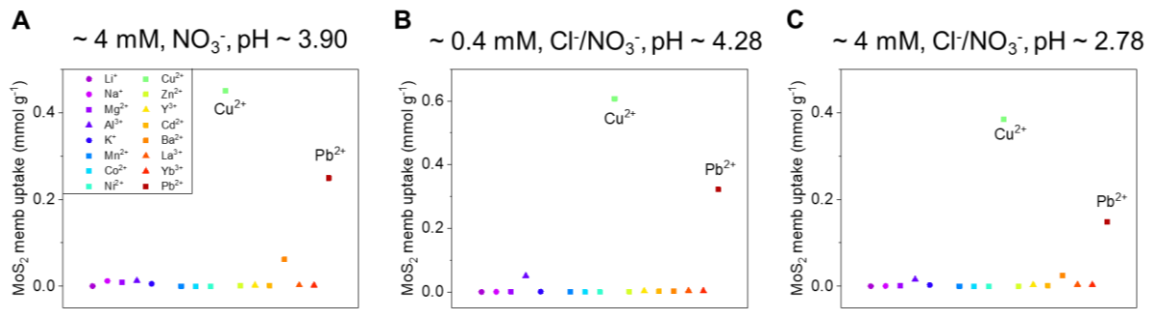


**Fig. S16 The anion effect, concentration effect and pH effect on the uptake of the metal cations in the  $\text{MoS}_2$  membrane.** (A) Uptake conditions: ~ 4 mM, pure  $\text{NO}_3^-$ , pH ~ 3.90. (B) Uptake conditions: ~ 0.4 mM,  $\text{Cl}^-/\text{NO}_3^-$ , pH ~ 4.28. (C) Uptake conditions: ~ 4 mM,  $\text{Cl}^-/\text{NO}_3^-$ , pH ~ 2.78. The absolute uptake of the metal cations in the  $\text{MoS}_2$  membrane are smaller than those of  $\text{MoS}_2\text{-COOH}$  membrane, which can be attributed to the blocked channels in the  $\text{MoS}_2$  membrane due to the intrinsically irreversible hydration/dehydration of the  $\text{MoS}_2$  membrane.

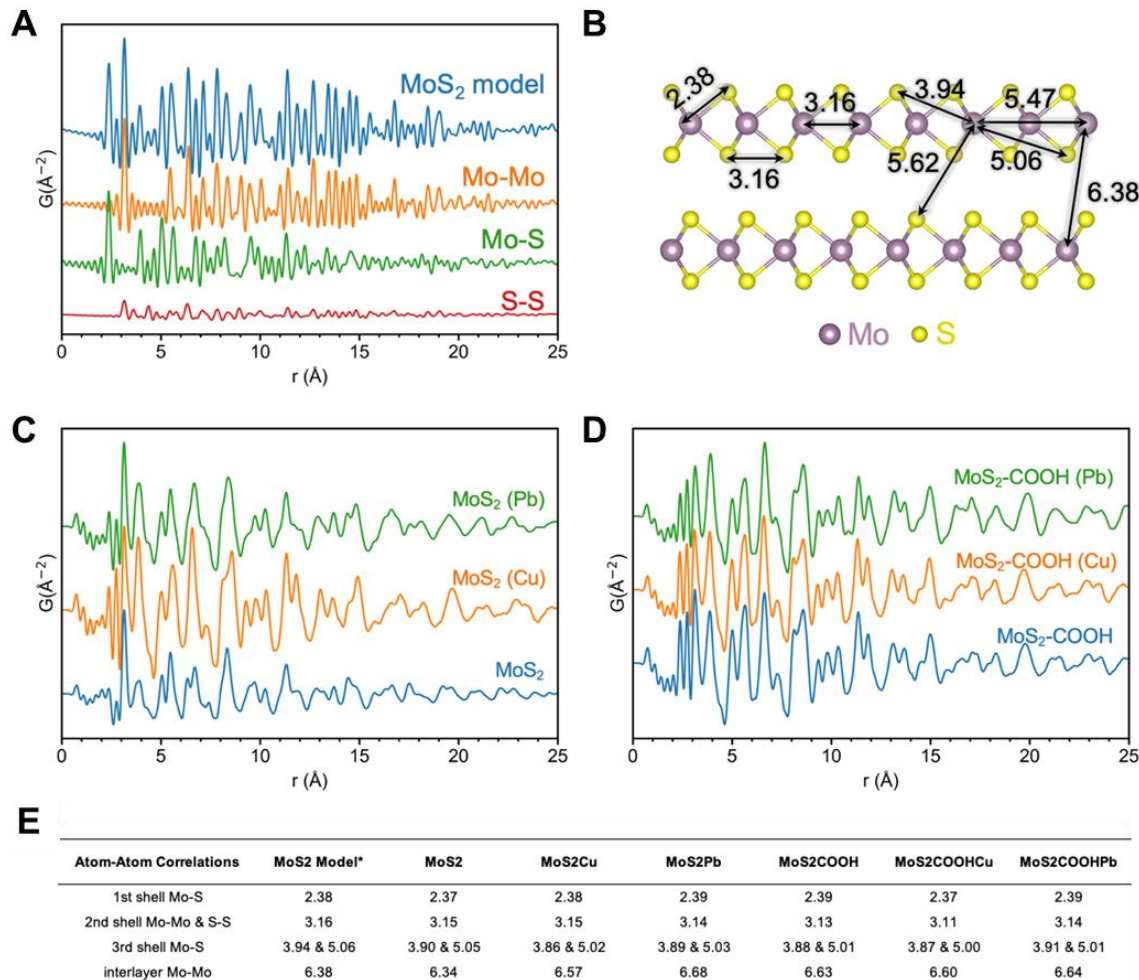


**Fig.S17 PDF analyses.** (A) PDFs of a MoS<sub>2</sub> model obtained from the crystallography open database (Entry 9007660); (B) Scheme of representative atomic distances in the MoS<sub>2</sub> model structure; (C) PDF comparison of MoS<sub>2</sub>, MoS<sub>2</sub>(Cu), and MoS<sub>2</sub>(Pb); (D) PDF comparison of MoS<sub>2</sub>-COOH, MoS<sub>2</sub>-COOH (Cu), and MoS<sub>2</sub>-COOH(Pb). (E) Summary of atomic distances (unit: Å). Note: \* MoS<sub>2</sub> model was obtained from the crystallography open database (Entry 9007660).

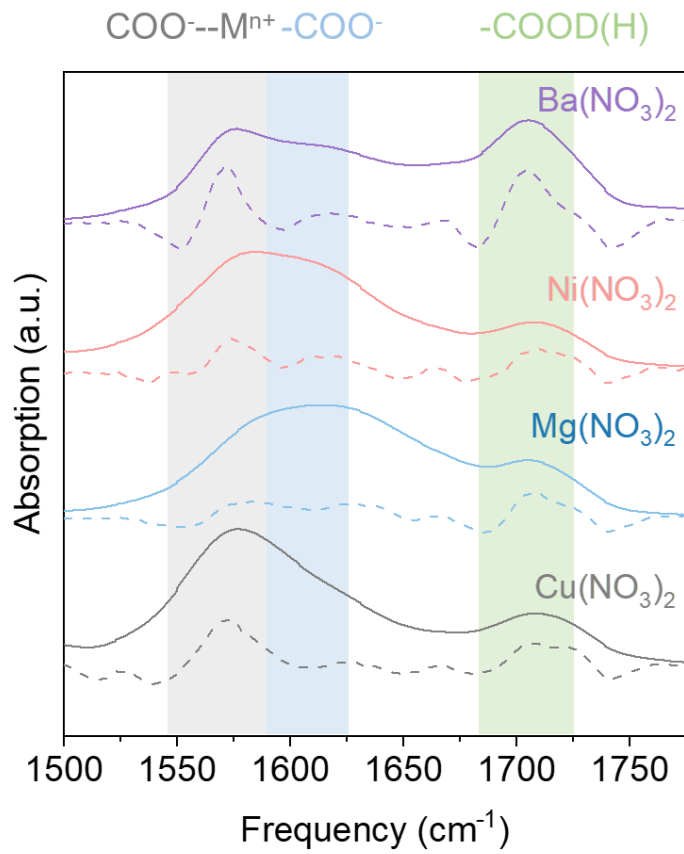


**Fig. S18** The effect of different metal cations on the IR absorption spectra of the carboxylate group in the MoS<sub>2</sub>-COOH membranes. The dashed lines are the corresponding negative second-order derivatives of the absorption spectra (solid lines) for peak pinpointing. Several salts of the same metal cation with different anions were measured for double-checking.

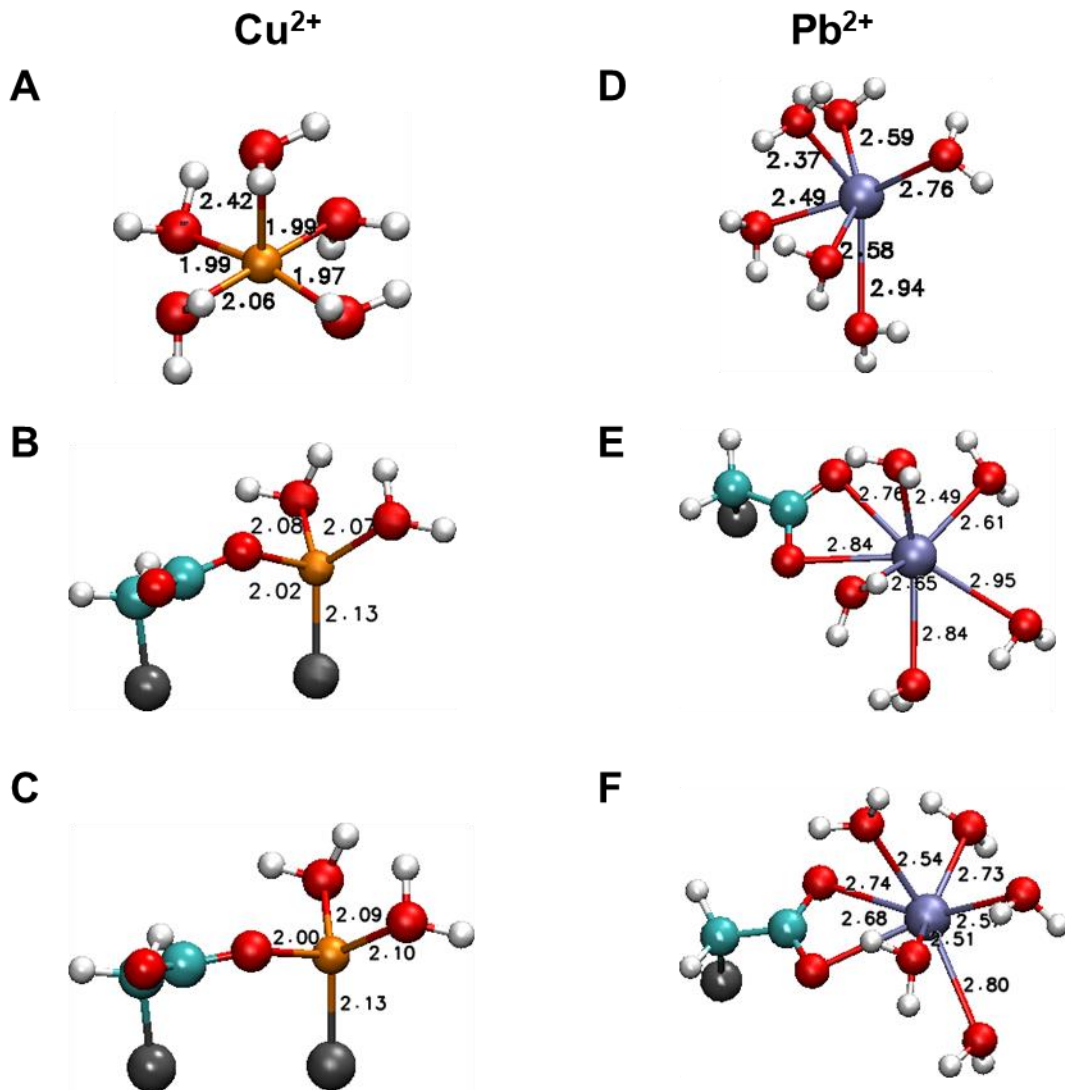


**Fig. S19 DFT calculations of the metal center binding corresponding to the optimized structure for Cu<sup>2+</sup> and Pb<sup>2+</sup> in the MoS<sub>2</sub>-COOH systems of Fig. 5 in the main text.** (A, B, C) Cu<sup>2+</sup> ion in the bulk solution, bound to monolayer and bilayer MoS<sub>2</sub>-COOH, respectively. (D, E, F) Pb<sup>2+</sup> ion in the bulk solution, bound to monolayer and bilayer MoS<sub>2</sub>-COOH, respectively. The number in each figure specifies the bond lengths (unit: Å). Mo is represented in yellow, S in gray, C in cyan, O in red, H in white, Cl in green, Cu in orange and Pb in ice blue.

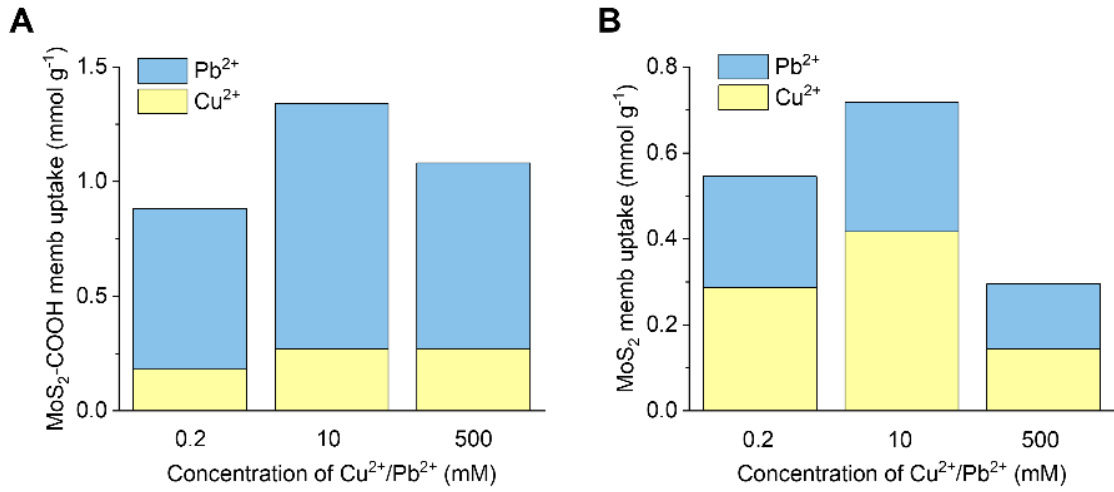


**Fig. S20 The uptake of MoS<sub>2</sub>-based membrane in the binary mixture solution of Cu<sup>2+</sup>/Pb<sup>2+</sup>.** (A) The uptake of MoS<sub>2</sub>-COOH membrane in the binary mixture Cu<sup>2+</sup>/Pb<sup>2+</sup> solution of different concentrations. (B) The uptake of MoS<sub>2</sub> membrane in the binary mixture Cu<sup>2+</sup>/Pb<sup>2+</sup> solution of different concentrations. All the salts are nitrate based. Note the dry degree of MoS<sub>2</sub> membranes used in (B) were not controlled to be the same. pH values: 0.2 mM Cu(NO<sub>3</sub>)<sub>2</sub>/Pb(NO<sub>3</sub>)<sub>2</sub> ~4.34; 10 mM Cu(NO<sub>3</sub>)<sub>2</sub>/Pb(NO<sub>3</sub>)<sub>2</sub> ~3.81; 500 mM Cu(NO<sub>3</sub>)<sub>2</sub>/Pb(NO<sub>3</sub>)<sub>2</sub> ~2.10.

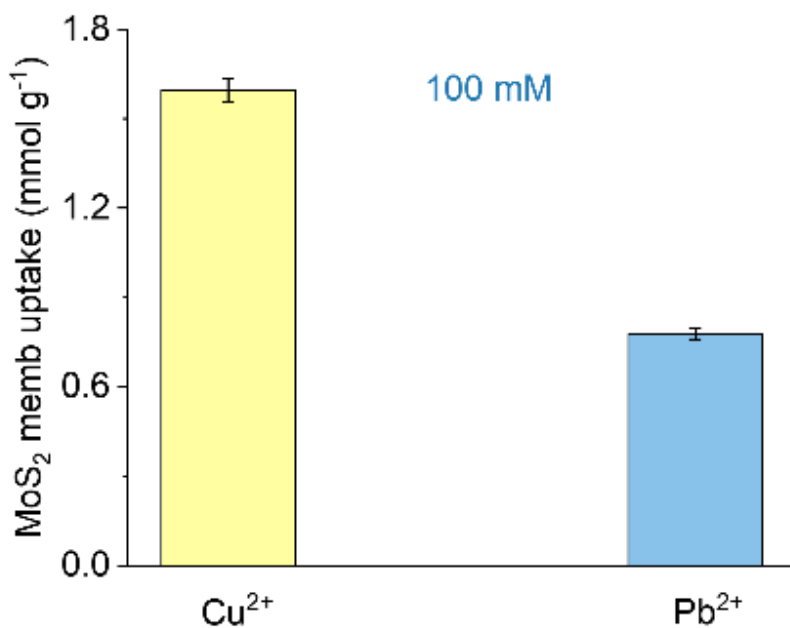


**Fig. S21 The uptake of  $\text{MoS}_2$  membrane in single metal cation solution (~100 mM).** pH values: 100 mM  $\text{Cu}(\text{NO}_3)_2 \sim 3.93$ ; 100 mM  $\text{Pb}(\text{NO}_3)_2 \sim 3.23$ . Note: The uptake of ions in the pristine  $\text{MoS}_2$  membrane is dependent on the drying degree of  $\text{MoS}_2$  membrane, while the drying of  $\text{MoS}_2$  membrane is not as controllable and reversible as that  $\text{MoS}_2\text{-COOH}$  membrane. To avoid the issue of  $\text{MoS}_2$  membrane with varied drying degrees, we prepared six  $\text{MoS}_2$  membrane and let them air dry simultaneously in the same condition at the same time for ~ 1 hour. Then three of them were used for single  $\text{Cu}^{2+}$  uptake and the left three were used for single  $\text{Pb}^{2+}$  uptake immediately.

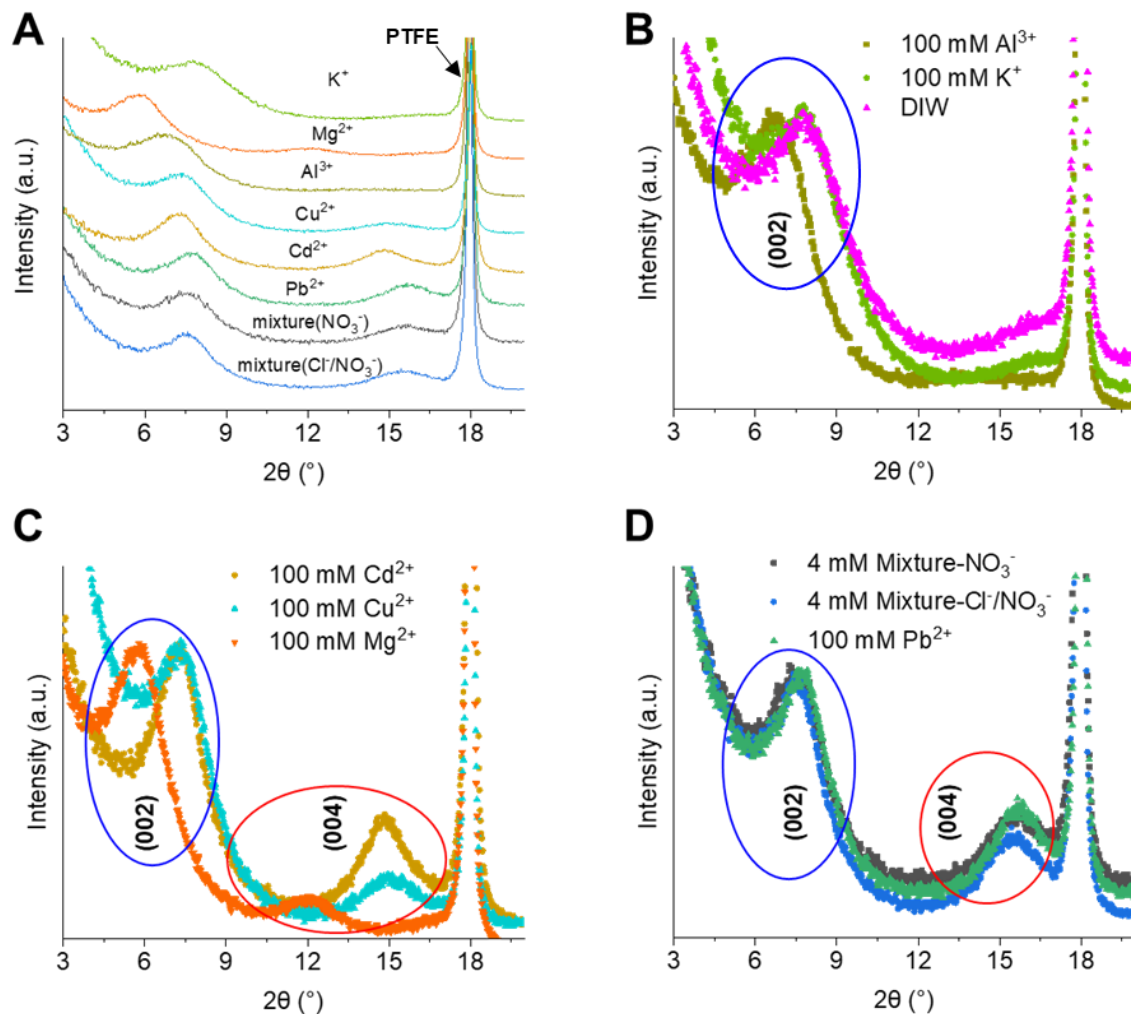


**Fig. S22 XRD spectra of the MoS<sub>2</sub>-COOH membranes.** (A) The XRD spectra of the MoS<sub>2</sub>-COOH membranes treated by different solutions. The concentration of the single salt solutions used is 100 mM (natural pH after salt dissolving in DI water) and all the salts are nitrate based. (B, C, D) show the same spectra in (A) and the replots are meant for better comparison. The blue circle indicates the (002) peak and the red circle indicates the (004) peak of the restacked MoS<sub>2</sub>-COOH membrane.

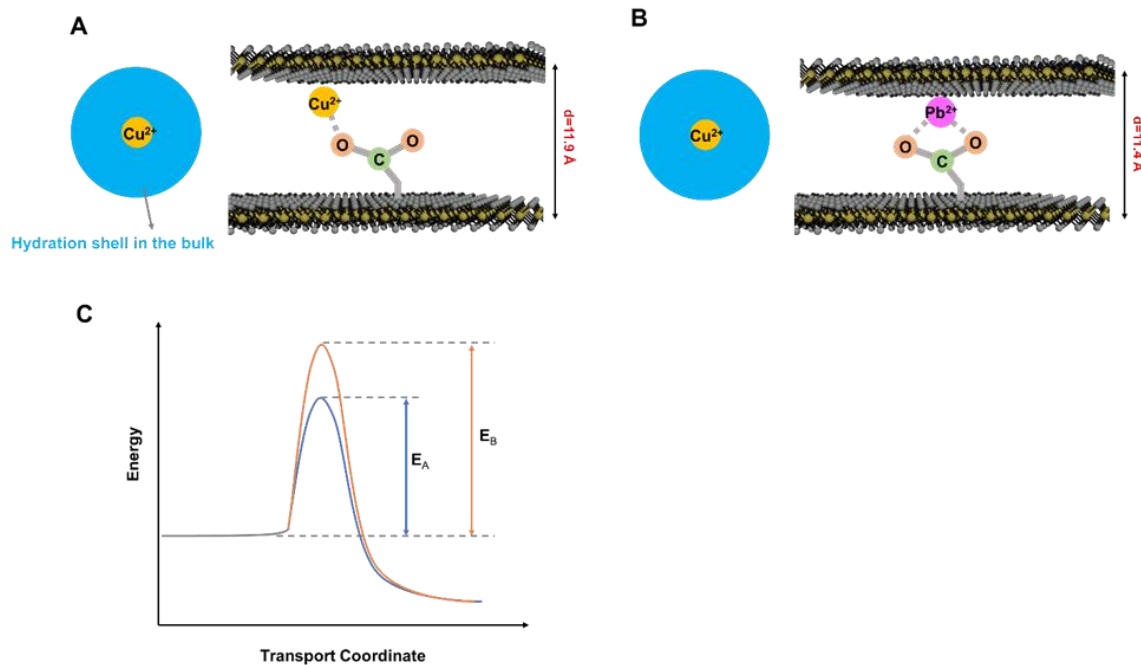


**Fig. S23 Kinetic energy barriers for  $\text{Cu}^{2+}$  uptake into the  $\text{Cu}^{2+}$ -locked  $\text{MoS}_2\text{-COOH}$  membrane and  $\text{Pb}^{2+}$ -locked  $\text{MoS}_2\text{-COOH}$  membrane.** (A) Schematic of the bulk  $\text{Cu}^{2+}$  uptake into the  $\text{Cu}^{2+}$ -locked  $\text{MoS}_2\text{-COOH}$  membrane. (B) Schematic of the bulk  $\text{Cu}^{2+}$  uptake into the  $\text{Pb}^{2+}$ -locked  $\text{MoS}_2\text{-COOH}$  membrane. (C) Energy diagram of  $\text{Cu}^{2+}$  uptake into the  $\text{Cu}^{2+}$ -locked  $\text{MoS}_2\text{-COOH}$  membrane and the  $\text{Pb}^{2+}$ -locked  $\text{MoS}_2\text{-COOH}$  membrane.  $E_A$  and  $E_B$  correspond to the kinetic barriers for bulk  $\text{Cu}^{2+}$  uptake into the  $\text{Cu}^{2+}$ -locked  $\text{MoS}_2\text{-COOH}$  membrane (A) and  $\text{Pb}^{2+}$ -locked  $\text{MoS}_2\text{-COOH}$  membrane (B). Since  $\text{Pb}^{2+}$ -locked  $\text{MoS}_2\text{-COOH}$  membrane has a smaller interlayer spacing than  $\text{Cu}^{2+}$ -locked  $\text{MoS}_2\text{-COOH}$  membrane ( $11.4\text{ \AA}$  vs  $11.9\text{ \AA}$ ),  $E_B$  is thus greater than  $E_A$ . This might explain why  $\text{Cu}^{2+}$  has a larger uptake in the single salt uptake tests while a smaller uptake in the mixture uptake tests, as compared to  $\text{Pb}^{2+}$ .

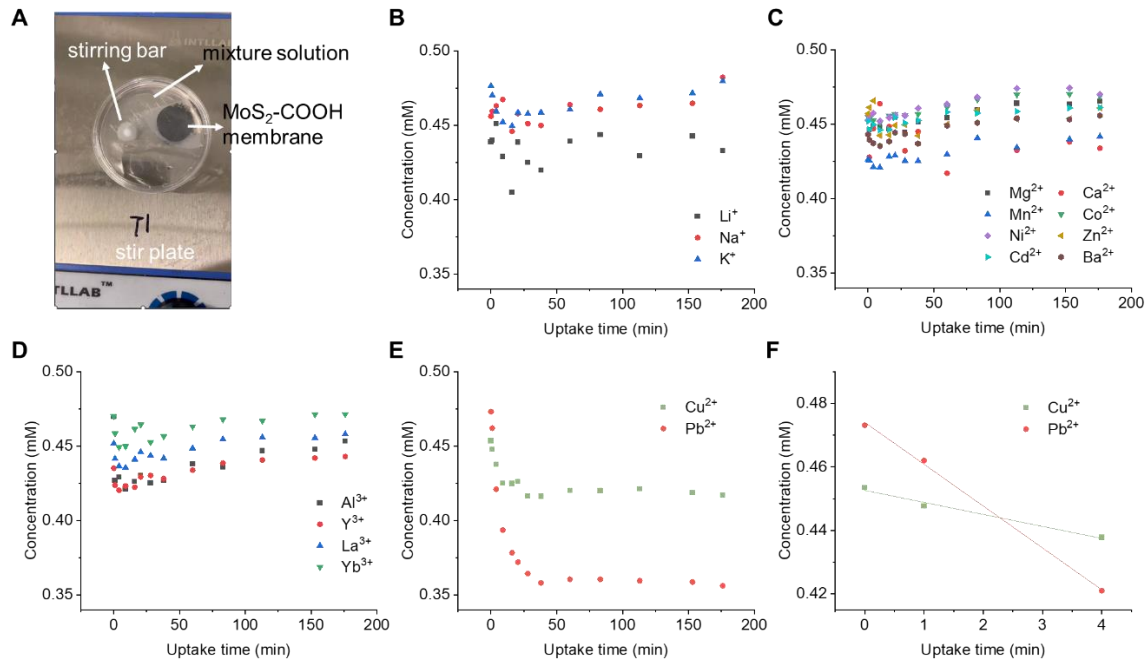


**Fig. S24 The uptake dynamics of ions in the MoS<sub>2</sub>-COOH membrane.** (A) Setup for dynamic membrane uptake test. (B-E) show the ion concentration profile of the solution throughout the test. (F) is the zoom-in plot of (E) showing that the uptake of Pb<sup>2+</sup> is faster than Cu<sup>2+</sup> (slope ratio Pb<sup>2+</sup>:Cu<sup>2+</sup>=3.5:1). (E, F) are shown as **Fig. 6B** and **C** in the main text, respectively.

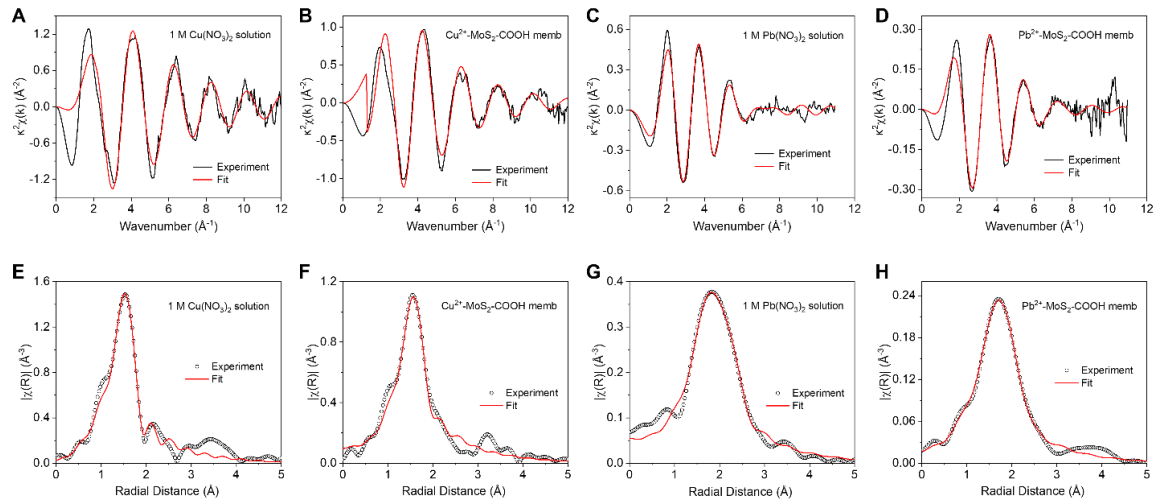


**Fig. S25 X-ray absorption spectroscopy (XAS) measurements.** Fourier transformed EXAFS spectra in the k-space of Cu K-edge for 1M  $\text{Cu}(\text{NO}_3)_2$  solution (A) and for  $\text{Cu}^{2+}$ -soaked  $\text{MoS}_2\text{-COOH}$  membrane (B) and of Pb L-edge for 1M  $\text{Pb}(\text{NO}_3)_2$  solution (C) and for  $\text{Pb}^{2+}$ -soaked  $\text{MoS}_2\text{-COOH}$  membrane (D). (E-F) are the Fourier transformed EXAFS spectra in the R-space corresponding to (A-D), respectively. Detailed data analyses are shown in **Table S3**. Data presented in **Fig. 6D** are a combination of **Figs. S25E** and **F**. Data presented in **Fig. 6E** are a combination of **Figs. S25G** and **H**.

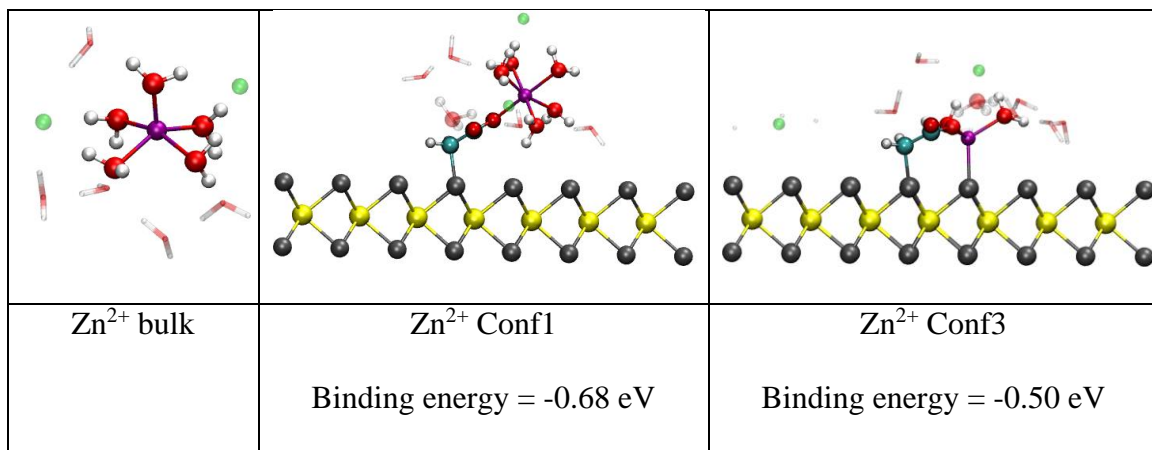


**Fig. S26** DFT calculated structures of the Zn<sup>2+</sup> metal center in the bulk and in monolayer MoS<sub>2</sub>-COOH systems at different configurations and their binding energies. Mo is represented in yellow, S in gray, C in cyan, O in red, H in white, Cl in green, and Zn in magenta.

**Table S1** The hydration radii and hydration enthalpies of metal cations

	Hydration radius (Å)	Hydration enthalpy (- kJ mol <sup>-1</sup> )	Bulk diffusion coefficient (10 <sup>-5</sup> cm <sup>2</sup> s <sup>-1</sup> )
<b>Li<sup>+</sup></b>	3.82	515	1.029
<b>Na<sup>+</sup></b>	3.58	405	1.334
<b>K<sup>+</sup></b>	3.31	321	1.957
<b>Mg<sup>2+</sup></b>	4.28	1922	0.706
<b>Ca<sup>2+</sup></b>	4.12	1592	0.792
<b>Ba<sup>2+</sup></b>	4.04	1304	0.847
<b>Mn<sup>2+</sup></b>	4.38	1845	0.712
<b>Co<sup>2+</sup></b>	4.23	2054	0.732
<b>Ni<sup>2+</sup></b>	4.04	2106	0.661
<b>Cu<sup>2+</sup></b>	4.19	2100	0.714
<b>Zn<sup>2+</sup></b>	4.3	2044	0.703
<b>Cd<sup>2+</sup></b>	4.26	1806	0.719
<b>Pb<sup>2+</sup></b>	4.01	1480	0.945
<b>Al<sup>3+</sup></b>	4.75	4660	0.541
<b>Y<sup>3+</sup></b>	/	3620	0.550
<b>La<sup>3+</sup></b>	4.52	3283	0.619
<b>Yb<sup>3+</sup></b>	4.65	3715	0.582

**Note:** The hydration enthalpies of the metal cations are taken from Ref. (46). We noticed that different measurements would often report different values of hydration radius even for the same cation, although they can show a consistent trend, namely the increased hydrated radius with respect to the increase of Lewis acidity of cations. Given the reported discrepancy of hydration radii of metal cations in different literatures, the hydration radii of the metal cations listed here are all adopted from Ref. 23 of the main text, for the sake

of consistency. In **Ref. 23** of the main text, the hydration radius value of  $\text{Y}^{3+}$  is missing, while  $\text{Yb}^{3+}$  is approximated by its neighboring lanthanides member  $\text{Tm}^{3+}$ . The bulk diffusion coefficients are taken from **Ref.** (44) of the Supplementary Reference.

**Table S2 XRD spectra analyses of the MoS<sub>2</sub>-COOH membranes treated by different solutions (single salt solution concentration ~ 4 mM, Fig.5A).**

samples	(002) peak		(004) peak		I(004)/I(002)	Interlayer spacing (Å)
	Position (2θ/°)	FWHM (°)	Position (2θ/°)	FWHM (°)		
MoS <sub>2</sub> bulk	14.38	0.17	29.02	0.2	0.023	6.2
MoS <sub>2</sub> -COOH memb air dry	8.59	2.44	/	/	/	10.3
MoS <sub>2</sub> -COOH memb DIW	8.02	2.92	/	/	/	11.0
MoS <sub>2</sub> -COOH memb-K <sup>+</sup>	7.96	2.86	/	/	/	11.1
MoS <sub>2</sub> -COOH memb-Mg <sup>2+</sup>	5.95	2.44	11.62	2.69	0.184	14.8
MoS <sub>2</sub> -COOH memb-Al <sup>3+</sup>	7.02	2.55	/	/	/	12.6
MoS <sub>2</sub> -COOH memb-Cu <sup>2+</sup>	7.44	2.27	14.98	1.96	0.144	11.9
MoS <sub>2</sub> -COOH memb-Cd <sup>2+</sup>	7.34	1.88	14.74	1.44	0.251	12.0
MoS <sub>2</sub> -COOH memb-Pb <sup>2+</sup>	7.76	1.85	15.62	1.67	0.306	11.4
MoS <sub>2</sub> -COOH memb-mixture (Cl <sup>-</sup> /NO <sub>3</sub> <sup>-</sup> )	7.72	1.80	15.17	1.61	0.336	11.4
MoS <sub>2</sub> -COOH memb-mixture (NO <sub>3</sub> <sup>-</sup> )	7.72	1.82	15.43	1.76	0.207	11.4

Note: (i) All the data were collected after the baseline subtraction of the raw figures. FWHM is short for full width at half maximum.

(ii) To avoid the variation in the qualitative analyses due to samples, the spectra in **Fig. 6A** and **Fig.S22** were collected from the same MoS<sub>2</sub>-COOH membrane cut into pieces for XRD tests.

**Table S3 EXAFS fitting parameters Cu K-edge and Pb L3-edge of the samples**

Sample	Bond	CN	error	R(Å)	error	E <sub>0</sub> (eV)	error	σ <sup>2</sup> (Å <sup>2</sup> )	error	R-factor
Cu <sup>2+</sup> solution	Cu-O	3	0.7	1.93	0.02	-1.7	2.2	0.0091	0.0087	0.014
	Cu-O	2	0.4	1.98	0.02	-1.7	2.2	0.0008	0.0022	
Cu <sup>2+</sup> -MoS <sub>2</sub> -COOH memb	Cu-O	2.1	0.2	1.97	0.03	6.2	2	0.0059	0.0076	0.015
	Cu-O	1.4	0.2	2.01	0.03	6.2	2	0.0064	0.0147	
Pb <sup>2+</sup> solution	Pb-O	1	0.1	2.35	0.03	-0.1	0.85	0.0054	0.0046	0.0078
	Pb-O	5	0.6	2.57	0.02	-0.1	0.85	0.0194	0.0044	
Pb <sup>2+</sup> -MoS <sub>2</sub> -COOH memb	Pb-O	0.6	0.1	2.32	0.03	-7	1.3	0.008	0.0031	0.015
	Pb-O	3.1	0.4	2.49	0.03	-7	1.3	0.0245	0.004	

Note: CN, coordination number; R, scattering length; E<sub>0</sub>, energy shift; σ<sup>2</sup>, Debye-Waller factor; R-factor, goodness of fitting.



Zn2+-bulk

1.000000000000000		
40.000000000000000	0.000000000000000	0.000000000000000
0.000000000000000	40.000000000000000	0.000000000000000
0.000000000000000	0.000000000000000	40.000000000000000

H O Cl Zn

20	10	2	1
----	----	---	---

Direct

0.4542833592494580	0.5184710223886100	0.5180639057555960
0.6038652804465480	0.4658090230472560	0.5193997014976190
0.5807177443062050	0.4946897475644930	0.5045719531751510
0.4902021058761500	0.5327797466878500	0.5266861496205090
0.4532139133666170	0.5516367048426570	0.4623827945379020
0.4802737446359080	0.5563492160411840	0.4345375287110890
0.5537977205939550	0.5440628074882590	0.4939244747762780
0.5925401479806850	0.5483552489264410	0.4883965573885970
0.4353397654558290	0.4460845581565490	0.5408348094799820
0.4674444004752720	0.4205331390958940	0.5499608188032070
0.5165219769192500	0.5836754916910110	0.5152144863216670
0.4999977410191640	0.5643421481383580	0.4843992164957310
0.5504988549681610	0.4736367700776960	0.5492115482259900
0.5258916425119150	0.4498130179535870	0.5693882384348180
0.4020123135684840	0.4839681402873380	0.5218971381238470
0.3975260112660870	0.4837835772144810	0.5606049281830600
0.4602597564457580	0.4880688477982810	0.4695677279396970
0.4832364125633850	0.4567301899447850	0.4595808826832330
0.5483080083917920	0.4402784600218220	0.5016205697873270
0.5243941176843940	0.4147459669217420	0.5204059100419010
0.4741189291117030	0.5149012387599040	0.5329816173647110
0.5807349047495970	0.4720186611614630	0.5154991100986230
0.4727845867491780	0.5656920341524480	0.4556928337623480
0.5746492185357890	0.5319921696332550	0.4874773362482610
0.4571531527058850	0.4361533066182940	0.5333328553411710
0.5156858621169880	0.5618902848638210	0.5044761477740560
0.5282244847436310	0.4733450848210760	0.5601024416159600
0.4003191504073760	0.4689662481710000	0.5415446542193010
0.4834615176813620	0.4783392404211490	0.4708136643370150
0.5256271572479670	0.4305949380326970	0.5007927565469430
0.5125556854114840	0.4011108769783070	0.5690851295103480
0.4192360230772960	0.5161818855426070	0.4804047850976400
0.4935243807367010	0.4682302105556810	0.5218572121004280









0.4531150228431640	0.6570000136036210	0.2283300259672670	0.2333145935572240	0.4462251608670440	0.3739578476541040
0.2911346631610030	0.5599338906704290	0.2216107074674480	0.2723171339596100	0.0770789678413379	0.2633940238616210
0.7655991125805590	0.7385759553186650	0.3021158550689900	0.3830282336293320	0.4625891656371830	0.4316424454666500
0.9023899904691670	0.8969467379357420	0.2513176816973010	0.3560797082103020	0.3876764913829830	0.3750624802189430
0.6826712001991090	0.7812077517934170	0.2686012860552220	0.3762097016612880	0.4124336730825880	0.2432495014617610
0.0435409059213114	0.9601401623975930	0.2527972958640770	0.5726837234085020	0.5514089434382610	0.2446019366266080
0.5617532029331110	0.8771579991235540	0.2905680061551470	0.3507910119164350	0.0934800654560419	0.2457672563923480
0.5584450011726780	0.7701158118987620	0.3277012400785670	0.5578766528806080	0.2063129322164130	0.3584997312504960
0.4228569484684780	0.0015049381818883	0.2704512312969880	0.3490631570524910	0.2593928584007080	0.3535385775747100
0.6449140144945170	0.7001485522435970	0.3892216411394140	0.7660611535367390	0.4443573365412660	0.263538766652930
0.5056654793206330	0.6302171124736510	0.3999500890939840	0.5946084996262750	0.1429080193189940	0.2478681120978900
0.4141954918043140	0.2376539684239910	0.3107007831888850	0.1525805797809090	0.3114083534249800	0.2634946903961430
0.2755600169163790	0.1293029042173040	0.2913929264127750	0.6071698025709790	0.4752875940754530	0.3623715805884580
0.3042201767513500	0.2742706775707260	0.2861844584405730	0.8195416559546580	0.6743422032341820	0.2443220253135650
0.6566715175948510	0.5757072625031010	0.2306773187950170	0.1508219626917500	0.4165855008545440	0.3560625337279850
0.3796872555446520	0.5670676839240300	0.2147982186388330	0.3676205209495430	0.4664971363396400	0.3905912430276990
0.3853281831009590	0.4637688628712970	0.2468788425338030	0.5324842050549200	0.3282510225326610	0.2810884720661440
0.2351492777070660	0.9663357553188940	0.2588717983324350	0.1162845177729530	0.073117799577213	0.2916842589723810
0.7999215535708750	0.6782128201785440	0.3736096799069910	0.4927968147142740	0.3022080215259700	0.4615664269652050







0.4911756244588830	0.6290145280773130	0.3958491569791530	0.5128769282947160	0.0269421312929694	0.3251581091416960
0.4223577915624970	0.2492239896550570	0.3218767284055130	0.1709673619855250	0.3306693259897950	0.2745998217409990
0.2852231513329570	0.1423006620922100	0.3026682808694400	0.5947521324077050	0.5257279134668940	0.3688880471629970
0.3145096382610930	0.2877434777548300	0.2977651693572410	0.8284978709209550	0.7004414705436870	0.2633343714508950
0.6691758112590020	0.5873065526140800	0.2380528024924110	0.1654264716235470	0.4839407858136010	0.3421145813778210
0.3938641226689150	0.5752981680821270	0.2238952034144850	0.3161201489521300	0.4151507931622680	0.3992349323675270
0.3974834234720670	0.4698225127339340	0.2537120615813530	0.5434674433586930	0.3533083308548370	0.3044089530083190
0.8088213632313090	0.6856201955720920	0.3669547900614770	0.1417275348538560	0.0931864296269396	0.2990681882405110
0.2474379063304960	0.9800528398806910	0.2701227709243590	0.4384498761912210	0.6663544266253180	0.3514921575969860

Input files:

**INCAR:**

```
SYSTEM = MoS2
ISTART = 0
ICHARG = 2
INIWAV = 1
NWRITE = 3
LWAVE = FALSE.
LCHARG = .FALSE.
PREC = Accurate
ENCUT = 520
NELM = 100
LREAL = Auto
#ALGO = Normal
#LSOL = .TRUE.
ISMEAR = 0
SIGMA = 0.01
# Prec = Low
ALGO = Fast
EDIFF = 1E-06
EDIFFG = -0.01
#IDIPOL = 3
#NSW = 200
IBRION = 2
#POTIM = 0.1
ISIF = 2
ISYM = 0
ISPIN = 2
NCORE = 8
IVDW = 12
```

**POTCARS:**

```
PAW_PBE Mo 08Apr2002
PAW_PBE S 17Jan2003
PAW_PBE C 08Apr2002
PAW_PBE H 15Jun2001
PAW_PBE O 08Apr2002
PAW_PBE Pb 08Apr2002
PAW_PBE Cl 17Jan2003
PAW_PBE Cu 05Jan2001
PAW_PBE Zn 06Sep2000
```

## References:

32. G. Kresse, D. Joubert, From ultrasoft pseudopotentials to the projector augmented-wave method. *Phys. Rev. B* **59**, 1758–1775 (1999).
33. J. Paier, R. Hirschl, M. Marsman, G. Kresse, The Perdew–Burke–Ernzerhof exchange–correlation functional applied to the G2-1 test set using a plane-wave basis set. *J. Chem. Phys.* **122**, 234102 (2005).
34. S. Grimme, J. Antony, S. Ehrlich, H. Krieg, A consistent and accurate *ab initio* parametrization of density functional dispersion correction (DFT-D) for the 94 elements H–Pu. *J. Chem. Phys.* **132**, 154104 (2010).
35. S. Grimme, S. Ehrlich, L. Goerigk, Effect of the damping function in dispersion corrected density functional theory. *J. Comput. Chem.* **32**, 1456–1465 (2011).
36. <https://webbook.nist.gov/cgi/cbook.cgi?ID=C1317404&Units=SI&Mask=FFFFI#Diatomc>.
37. <https://labs.chem.ucsb.edu/zakarian/armen/11---bonddissociationenergy.pdf>.
38. B. H. Toby, R. B. Von Dreele, GSAS-II : the genesis of a modern open-source all purpose crystallography software package. *J. Appl. Crystallogr.* **46**, 544–549 (2013).
39. P. Juhás, T. Davis, C. L. Farrow, S. J. L. Billinge, PDFgetX3 : a rapid and highly automatable program for processing powder diffraction data into total scattering pair distribution functions. *J. Appl. Crystallogr.* **46**, 560–566 (2013).
40. B. Schönfeld, J. J. Huang, S. C. Moss, Anisotropic mean-square displacements (MSD) in single-crystals of 2 *H* - and 3 *R* -MoS<sub>2</sub>. *Acta Crystallogr. B* **39**, 404–407 (1983).
41. P. Juhás, C. L. Farrow, X. Yang, K. R. Knox, S. J. L. Billinge, Complex modeling: a strategy and software program for combining multiple information sources to solve ill posed structure and nanostructure inverse problems. *Acta Crystallogr. Sect. Found. Adv.* **71**, 562–568 (2015).
42. S. Letourneau, *et al.*, Structural Evolution of Molybdenum Disulfide Prepared by Atomic Layer Deposition for Realization of Large Scale Films in Microelectronic Applications. *ACS Appl. Nano Mater.* **1**, 4028–4037 (2018).
43. S.-J. Hwang, V. Petkov, K. K. Rangan, S. Shastri, M. G. Kanatzidis, Structure of Nanocrystalline Materials with Intrinsic Disorder from Atomic Pair Distribution Function Analysis: The Intercalation Compound Ag<sub>x</sub>MoS<sub>2</sub>. *J. Phys. Chem. B* **106**, 12453–12458 (2002).

44. , "Ionic conductivity and diffusion at infinite dilution", in CRC Handbook of Chemistry and Physics, Internet Version 2005, David R. Lide, ed., <<http://www.hbcpnetbase.com>>, CRC Press, Boca Raton, FL, 2005.
45. I. A. Stenina, Ph. Sistat, A. I. Rebrov, G. Pourcelly, A. B. Yaroslavtsev, Ion mobility in Nafion-117 membranes. *Desalination* **170**, 49–57 (2004).
46. G. Wulfsberg, *Principles of Descriptive Chemistry*, Cole Publishing, (1987).